Journal of Structural Geology 157 (2022) 104568

Contents lists available at ScienceDirect

Journal of Structural Geology

journal homepage: www.elsevier.com/locate/jsg

Virtual outcrop models: Digital techniques and an inventory of structural models from North-Northwest Iberia (Cantabrian Zone and Asturian Basin)

Hodei Uzkeda [a], Josep Poblet [b,*], Marta Magán [b], Mayte Bulnes [b], Santiago Martín [c], David Fernández-Martínez [b]

[a] Terractiva, Ronda Sant Pere 52, 08010, Barcelona, Spain, EU
[b] Departamento de Geología, Universidad de Oviedo, C/Jesús Arias de Velasco s/n, 33005, Oviedo, Spain, EU
[c] Departamento de Construcción e Ingeniería de Fabricación, Universidad de Oviedo, Campus de Viesques, Edificio Departamental 6, 33203, Gijón, Spain, EU

ARTICLE INFO

Keywords:
Virtual outcrop model (VOM)
Digital geological mapping
Google Earth
Photogrammetry
Cantabrian Zone
Asturian Basin

ABSTRACT

The first steps to study natural structures are data collection, their representation and their geological interpretation. There is no doubt that the development of digital techniques in recent times has facilitated these tasks. Here we present an inventory of virtual outcrop models from the Cantabrian Zone and Asturian Basin, North-Northwest Iberian Peninsula, and the procedure employed to obtain the data, construct the models and interpret them geologically. These models correspond to contractional folds and faults of Palaeozoic age, and to Mesozoic extensional structures affected by Cenozoic tectonic inversion in the form of folds and thrusts. The digital techniques and data employed are fieldwork, as well as Google Earth images, orthophotographs, stereoscopical pairs of photographs and virtual outcrop models, constructed using Structure from Motion photogrammetry based on images extracted from Google Earth or from photographs taken in the field using a tripod or unmanned aerial vehicles. The analysis of these models has provided us with geological information that would have been difficult to obtain using traditional techniques. Apart from their scientific interest, the examples shown may be helpful for structural geologists who wish to obtain 3D geological models, maps and sections, and additional structural information from field examples, as well as elements to prepare a virtual fieldtrip and/or for educational purposes.

1. Introduction

Structural Geology may be defined as the branch of Geology that deals with the study of structures from the geometrical, kinematical and mechanical point of view, as well as with the causes, processes and conditions of their formation. Collecting structural data, as well as the graphical representation of the structures and their interpretation, using geological mapping techniques, remote sensing, etc., are the first steps to be taken when studying natural structures in the field, especially mesoscopic- and macroscopic-scale structures, the ones that concern us here. Similarly to the rest of scientific disciplines, these geological techniques have not been alien to technical advances in society, but have benefited from them and this has allowed a remarkable scientific improvement of Structural Geology over time. Advances have taken place on many fronts. Thus, in the early days of Structural Geology, for instance, only field data collected in situ were available, which were reflected in drawings made manually in a field notebook. The advances in the Earth visualization gave a great impulse to Structural Geology both in terms of representing structural data and to obtain additional data; thus, nowadays extremely accurate topographic maps, aerial photographs, orthophotographs, satellite images, digital elevation models (DEM), and Google Earth and Street View images are available. The instruments that structural geologists use to carry out fieldwork have also undergone an enormous change from analog compasses to compasses capable of storing data, Global Positioning Systems (GPS), Personal Digital Assistants (PDA), mobile phones and tablets, and from conventional photographic cameras to digital cameras and laser scanners. It goes without saying that computers have been a huge leap for society. In the field of Structural Geology, they initially allowed graphical representations of structures using drawing software packages with the advantages that this entailed, but later, powerful hardware and specific software have been available for the representation and

* Corresponding author.
E-mail addresses: hodei@terractiva.net (H. Uzkeda), jpoblet@geol.uniovi.es (J. Poblet), maganmarta@uniovi.es (M. Magán), maite@geol.uniovi.es (M. Bulnes), martinsantiago@uniovi.es (S. Martín), UO210262@uniovi.es (D. Fernández-Martínez).

https://doi.org/10.1016/j.jsg.2022.104568
Received 13 July 2021; Received in revised form 20 January 2022; Accepted 4 March 2022
Available online 8 March 2022

interpretation of structures, as well as for the management and processing of large amounts of structural data, such as Geographical Information Systems (GIS), numerical modelling software, etc. This continuous process of improvement over time has undergone significant leaps at certain times. Deciding which have been the most notable improvements is probably subjective and surely depends on the personal view of each one influenced by his research lines. As an example, we can mention an important step forward for Structural Geology in the sixties due to the quantification of parameters derived from the analysis of photogeological interpretations and geological sections across natural structures lead by the work of John G. Ramsay in 1967. From our point of view, the most important leap in the last decades has been the move from the 2D study of structures to have 3D data accompanied by digital support. Computer-assisted, three-dimensional techniques have become enormously popular in recent times.

The rise of these techniques has led to the creation of virtual outcrop models (VOM) all over the world (e.g., Xu et al., 2000). See for instance the open-access online repositories of VOMs called eRock (https://www.e-rock.co.uk) (Cawood and Bond, 2019) or Virtual 3D Geoscience (https://v3geo.com) (Buckley et al., 2021). Some regions of the planet have a large number of VOMs, while others are quite the opposite despite the growing expansion of these techniques. The north-northwest of the Iberian Peninsula corresponds to the latter case, although the creation of VOMs would be especially useful because it is a mountainous region with difficult access areas and where some outcrops are difficult to visualize because they are located in steep slopes (Fig. 1). The rainfall index recorded in the north-northwest of the Iberian Peninsula makes that many rock outcrops are covered by vegetation and soils, however, there are two sectors within this region where spectacular outcrops occur. The first of these areas is the coast, where high cliffs adjacent to the beaches occur because the submarine abrasion platform was raised in relatively recent times revealing spectacular outcrops (e.g., Flor, 1983; Mary, 1983). The second area is the Cantabrian Mountains (e.g., Alonso et al., 1996), that are roughly parallel to the coast and whose southern slope, adjacent to the central Spanish Plateau, exhibits an appropriate climate to preserve the outcrops. The tectonics suffered by this region gave rise to two main structural units (Fig. 1): the Cantabrian Zone, which is the foreland fold and thrust belt of the Variscan orogen of Palaeozoic age (Lotze, 1945; Julivert et al., 1972), and the Asturian Basin, a Permian-Mesozoic extensional basin inverted during the Alpine orogeny of Cenozoic age (e.g., García-Ramos and Gutiérrez-Claverol, 1995) that gave rise to the Cantabrian Mountains and the Pyrenees. Thus, this complex structural history makes the north-northwest portion of the Iberian Peninsula an exceptional natural laboratory made up of very different types of structures. We will show here an inventory of available VOMs of structures in this region (Fig. 1); they correspond to different examples of Variscan contractional structures and also to different types of Mesozoic extensional structures reactivated as reverse structures during the Alpine event. All the outcrops shown correspond to regions located on steep slopes prone to rock fall, inaccessible areas or regions only visible during low tide periods. Some of these models are shown and described here for the first time, while new descriptions are offered for others previously presented. Since these models were created employing different digital techniques, such as photogrammetry, VOMs, orthophotographs and stereoscopical pairs of photographs, together with conventional and digital mapping, we will explain the general guidelines used and the results obtained. We would like to make it clear that this work is not intended to be an exhaustive review of all the digital techniques, but rather to present the models available up to now, describe them and explain the various procedures employed to build them introducing a few technical innovations.

2. Methodology employed

2.1. Digital and "traditional" fieldwork

Nowadays, there are two different ways to collect data from outcropping structures: digital techniques and traditional methods. From our point of view, digital fieldwork has got some advantages over traditional fieldwork, however, it has also got some disadvantages. The strong points are: a) faster data acquisition; b) easier positioning of the collected data (at least in areas with good GPS coverage); c) ability to carry multiple types of supports such as maps, orthophotographs, etc.; and d) seamless transfer of field data to software back in the laboratory to backup and update older versions of maps. The most remarkable drawbacks are: a) some electronic devices provide good orientation and location measurements while others do not, b) excessive light on sunny days makes the screen of many mobile phones or tablets difficult to read, c) the electronic devices must be adequately waterproof protected in the event of heavy rains and/or fall into the water, d) the breakage of the

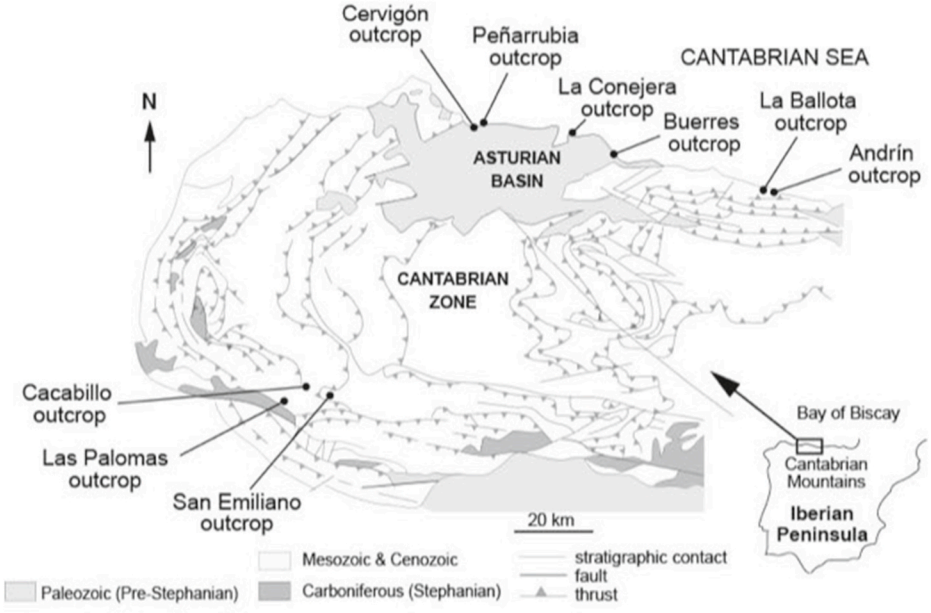

Fig. 1. Structural sketch of the north-northwest portion of the Iberian Peninsula showing the two main structural units (Cantabrian Zone and Asturian Basin) as well as the location of the virtual outcrops illustrated in the following figures.

mobile phone or tablet may cause the loss of the collected data, e) satellite coverage is poor in lush forests and in the lower part of steep slopes so that the location data provided by the mobile phones or tablets are not reliable, f) electronic devices must be periodically calibrated using an analog compass to ensure that the measurements are correct, and g) electronic devices are strongly conditioned by the duration of the batteries.

Irrespective of the types, features and scales of the studied structures, we carried out traditional fieldwork to collect new data as input data for the virtual models presented below. Fieldwork was also helpful to refine and improve the accuracy of the elements mapped in the laboratory and to check the results obtained from the digital techniques described in the following sections.

To improve the data collection procedure, as well as the process of integrating field data with data obtained in the laboratory, we collected field data using mobile phones and tablets (e.g., Allmendinger et al., 2017; Novakova and Pavlis, 2017, 2019) running a field-oriented application such as FieldMove (https://www.petex.com/products/move-suite/digital-field-mapping/), which can be downloaded for free, and ArcPad (https://www.esri.com/content/dam/esrisites/sitecore-archive/Files/Pdfs/library/brochures/pdfs/arcpadbro.pdf). These devices were used in combination with a high precision GPS when we thought the location data provided by our mobile phones or tablets were not sufficiently accurate. FieldMove and ArcPad allowed us to store in the mobile phones and tablets all sorts of information such as geographical coordinates, as well as dips and strikes, of stratigraphic contacts, faults, fold elements, etc. The collected data were imported into different types of supports such as aerial photographs, Google Earth images, VOMs, etc., using general software such as GIS, and more specific software such as an academic license of Move (https://www.petex.com/products/move-suite/), although other software with similar functionalities such as Andino 3D (https://www.andino3d.com.ar) may be used.

2.2. Google Earth

Two digital methods used to map large-scale structures are: the stereoscopic visualization of pairs of aerial and/or satellite photographs and their photogeological interpretation using specific software (e.g., Berger et al., 1992; Dueholm et al., 1993), and remote geological mapping from orthophotographs draped over DEM's managed using GIS software (e.g., Banerjee and Mitra 2004; Dhont et al., 2005). These two methods provide excellent results but do not seem to be the most widely used methods today. Anyway, these methods can be used in a complementary way to the most popular method nowadays which is Google Earth (https://www.google.com/earth/) (e.g., Lisle, 2006; Blenkinsop, 2012; Tavani et al., 2014; Martín et al., 2019; Wellmann et al., 2019). The main advantages of Google Earth with respect to the methods mentioned above are: a) Google Earth does not require the use of specific software for image visualization and/or interpretation because it provides its own free software; b) Google Earth has images of the entire planet for free, and therefore, there is no need to search for aerial photographs, orthophotographs, satellite images or DEM's of the region to be studied, difficult and/or expensive to get in some places; c) there is no need to worry about the scale of the photographs, orthophotographs, satellite images or DEM's as Google Earth allows zooming in and out the

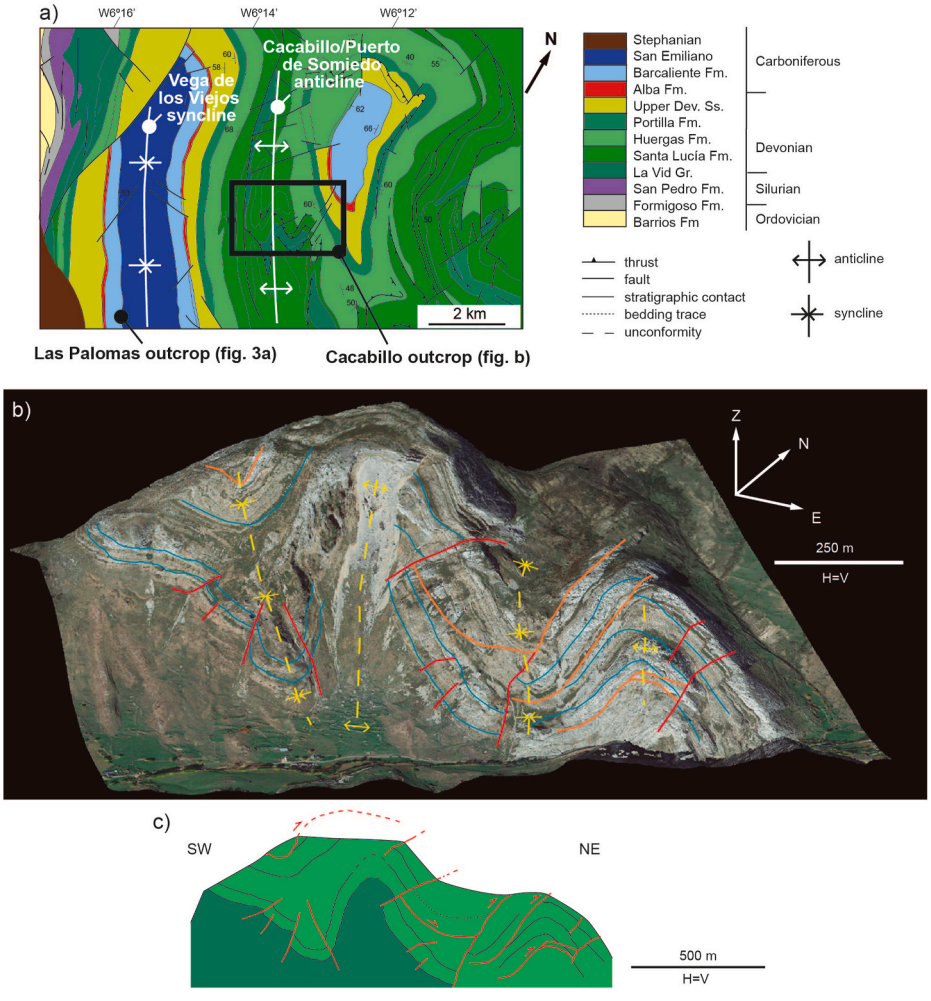

Fig. 2. Cacabillo outcrop. a) Geological map of the region where the virtual outcrops illustrated in figures b) and 3a are located showing the Cacabillo/Puerto de Somiedo anticline and the Vega de Los Viejos syncline (modified from Bastida et al., 1984), b) geological interpretation of a point cloud constructed using images from Google Earth (Martín et al., 2019), and c) geological cross-section obtained from the projection of the geological interpretation onto a plane (modified from Martín et al., 2019). See Fig. 1 for location. The latitude and longitude values of an approximately central point within the VOM are 42.9941°N and 6.1945°W respectively. (For interpretation of the references to colour in this figure legend, the reader is referred to the Web version of this article).

images without quality loss unless detailed images of small outcrops are needed; and d) Google Earth allows sharing the information easily. Thus, this set of reasons led us to use Google Earth.

The interpretation of geological structures using Google Earth was carried out employing elements implemented in this software such as linear features (e.g., intersection of lithological contacts with the topographic surface, fold and fault traces, lineaments), polygons (e.g., regions where a particular rock unit crops out, fault-damage zones) and points (e.g., dip/strike data, position of geological sketches and photographs) (Fig. 2b). All these elements were exported as kml files and loaded in a GIS software to create geological maps. One drawback derived from the geological interpretations carried out using Google Earth was that they lack altitude information, which was not a problem for generating maps, but limited its use, for instance, to calculate dips and strikes of bedding, faults, etc. This problem was overcome using auxiliary tools such as the free, online applications GPS Visualizer (https://www.gpsvisualizer.com) and KML Altitude Filler (https://www.nearby.org.uk/elevation-kml.php) that, amongst other aspects, allowed calculating altitudes for kml files exported from Google Earth. Another solution we carried out was building a VOM using images and points of known coordinates extracted from Google Earth (e.g., Martín et al., 2019). The procedure of constructing and interpreting a VOM derived from Google Earth images is described below.

The use of Google Earth is an excellent technique, however, we needed better resolutions, better points of view and more powerful zoom in/out factors than the ones provided by Google Earth to study mesoscopic geological structures developed in inaccessible areas. Due to these reasons, we used the additional digital techniques described below.

2.3. VOMs

Nowadays, 3D photorealistic VOMs are probably the most commonly used approaches to analyse outcrops from the geological point of view (e.g., Xu et al., 2000, 2001; Buckley et al., 2008; Hodgetts, 2013). The acquisition of the required data can be made by employing Light Detection and Ranging (LIDAR)/terrestrial laser scanners (TLS) (e.g., Pringle et al., 2004; Bellian et al., 2005; Trinks et al., 2005; McCaffrey et al., 2010) or, alternatively, using photogrammetry (e.g., Bemis et al., 2014; Svennevig et al., 2015; Corradetti et al., 2017; Sørensen and Dueholm, 2018; Sørensen and Guarnieri, 2018; Martín et al., 2019). We used the latter technique to create our VOMs because it is cheaper. Thus, the first method requires sophisticated devices, whereas the second can be carried out with commonly available devices such as photographic cameras and computers amongst others. Below we describe the practices we carried out for collecting the necessary data, as well as building and interpreting the VOMs.

2.3.1. Photogrammetry data collection

To generate our VOMs we used the structure from motion (Sfm) photogrammetry (Carrivick et al., 2016 and references therein), which is a relatively quick and unexpensive technique, and one of the most widely used. In the case of large-scale structures, we saved in our computer different Google Earth images to cover the area of interest (Fig. 2b). On the contrary, in the case of smaller-scale structures, we took several photographs using photographic cameras mounted on tripods for ground-based studies (Figs. 3a, 4b, 5b, 6a, 7c and 8b) and/or attached to unmanned aerial vehicles (UAV, drones) (Fig. 9a). UAVs were used when the outcrop met certain particularities such as: a) relatively large area to cover, as flying was faster than walking and, in some cases, recording a video at high frames per second (fps) rates and extracting selected frames was good enough for building a VOM (Li et al., 2018); b) outcrops whose geometry could only be properly captured from the air, such as vertical or steeply inclined cliffs and slopes whose height did not allow correct coverage photographing from ground level, or studies that required a top-down view of the terrain because the plunge of the structures was oblique to the topographic surface; and/or c) areas with environmental hazards, such as falling of rocks, slippery floor, etc., where getting close to the outcrop was not safe. Ground-based studies were used when: a) the outcrop to be simulated was relatively small; b) minor structures such as small veins, joints, cracks, etc. needed to be captured and handheld cameras yielded better pictures of these minor structures in terms of sharpness, resolution and contrast than cameras mounted on UAV's; c) the outcrop had relatively low relief, it was accessible and hiking was easy and safe, and therefore, it was easier to get close enough to the outcrop walking than piloting an

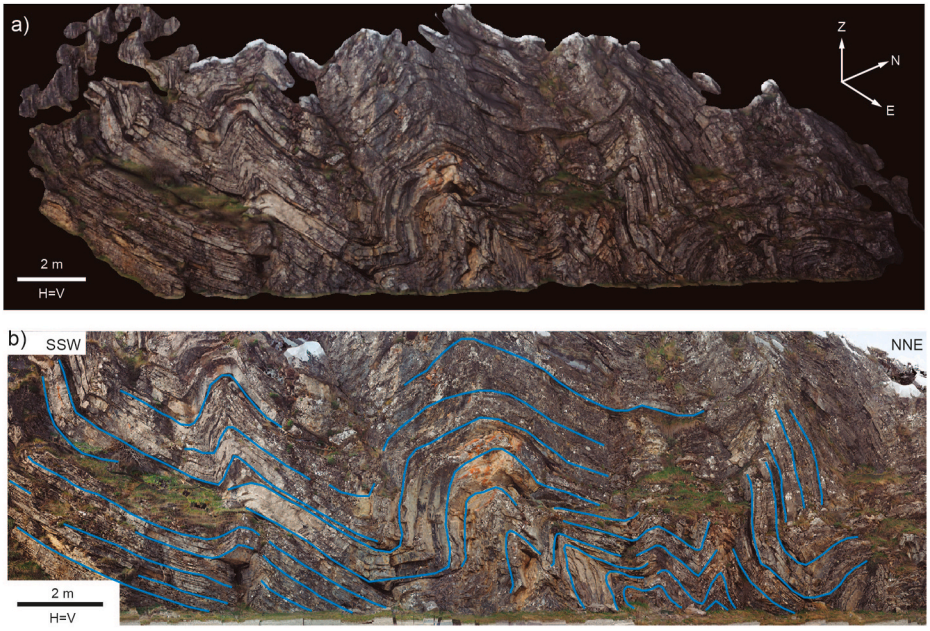

Fig. 3. Las Palomas outcrop. a) Triangular textured mesh showing the outcrop obtained using a photographic camera mounted on a tripod, and b) geological cross-section derived from the geological interpretation of an orthophotograph of the outcrop. See Figs. 1 and 2a for location. The latitude and longitude values of an approximately central point within the VOM are 42.9513°N and 6.2147°W respectively.

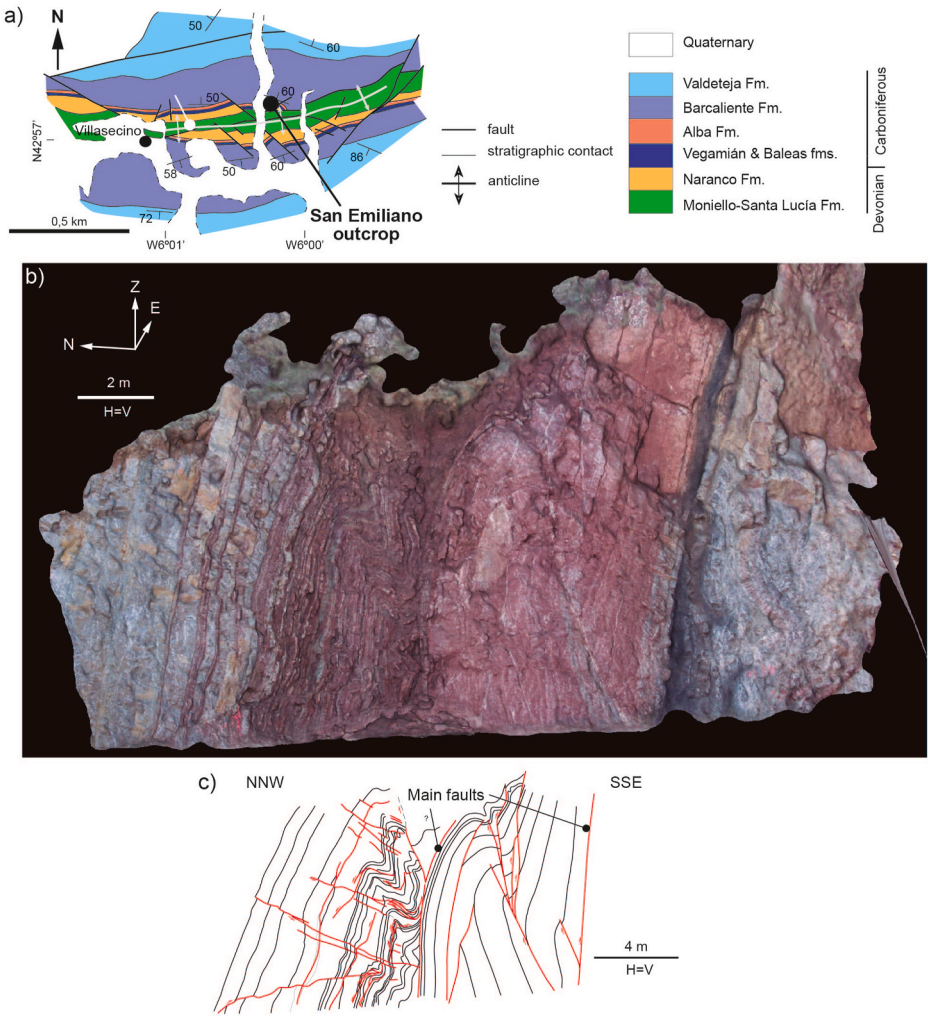

Fig. 4. San Emiliano outcrop. a) Geological map of the region where the virtual outcrop illustrated in figure b) is located showing the Huergas-Valgrande/Villasecino anticline (modified from Suárez-Rodríguez et al., 1991), b) triangular textured mesh showing the outcrop obtained using a photographic camera mounted on a tripod, and c) geological cross-section obtained from the projection of the geological interpretation onto a plane. See Fig. 1 for location. The latitude and longitude values of an approximately central point within the VOM are 42.9548°N and 6.0025°W respectively. (For interpretation of the references to colour in this figure legend, the reader is referred to the Web version of this article).

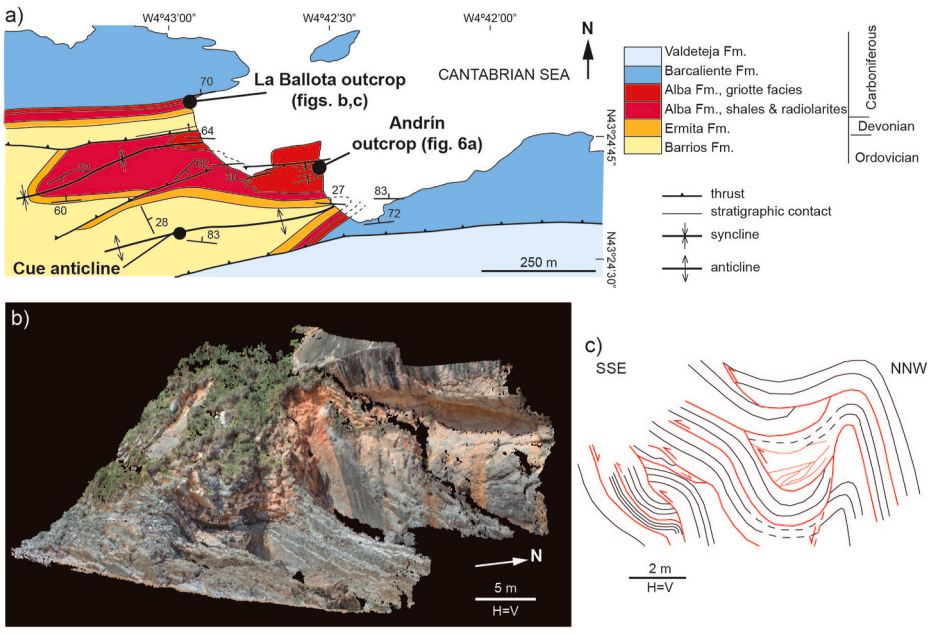

Fig. 5. La Ballota outcrop. a) Geological map showing the Cue anticline (modified from De Ana, 2015) and the region where the virtual outcrops illustrated in figures b) and 6a are located, b) point cloud showing the outcrop obtained using a photographic camera mounted on a tripod, and c) geological cross-section obtained from the projection of the geological interpretation onto a plane. See Fig. 1 for location. The latitude and longitude values of an approximately central point within the VOM are 43.4138°N and 4.7147°W respectively. (For interpretation of the references to colour in this figure legend, the reader is referred to the Web version of this article).

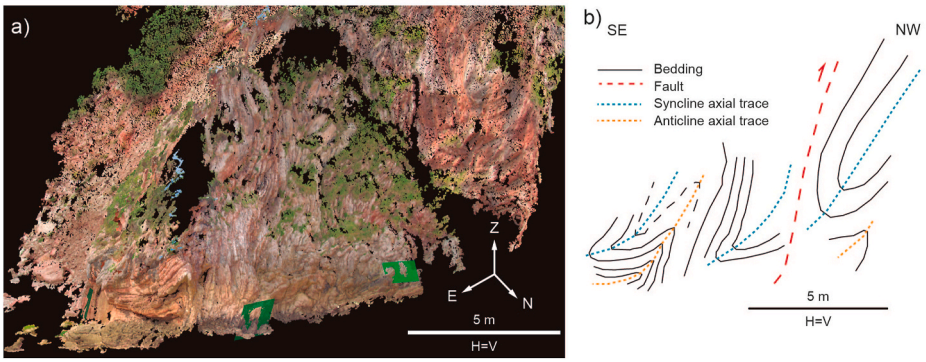

Fig. 6. Andrín outcrop. a) Point cloud showing the outcrop obtained using a photographic camera mounted on a tripod (Martín et al., 2019), and b) geological cross-section obtained from the projection of the geological interpretation onto a plane. See Figs. 1 and 5a for location. The latitude and longitude values of an approximately central point within the VOM are 43.4123°N and 4.7096°W respectively. (For interpretation of the references to colour in this figure legend, the reader is referred to the Web version of this article).

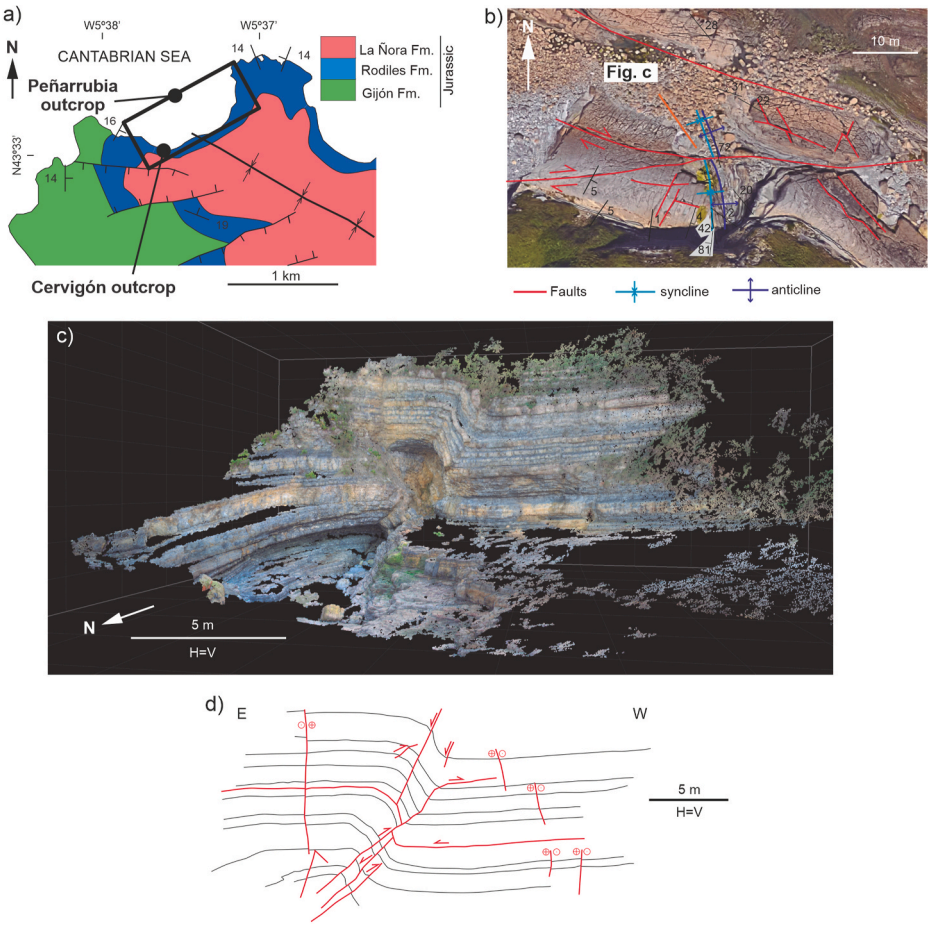

Fig. 7. Cervigón outcrop. a) Structural sketch showing the regional-scale structure where the virtual outcrops illustrated in figures c) and 9 are located (modified from Beroiz et al., 1972b), b) geological interpretation of an orthophotograph of the region where the virtual outcrop shown in figure c) is located (modified from Uzkeda et al., 2018), c) point cloud showing the outcrop obtained using a photographic camera mounted on a tripod (Uzkeda et al., 2018), and d) geological cross-section obtained from the intersection of 3D geological surfaces with a plane (modified from Uzkeda et al., 2018). The small red circles next to the fault surfaces in figure c) indicate strike-slip motion along the faults. See Fig. 1 for location. The latitude and longitude values of an approximately central point within the VOM are 43.5501°N and 5.6296°W respectively. (For interpretation of the references to colour in this figure legend, the reader is referred to the Web version of this article).

UAV; and/or d) the outcrop was located in an area where flying was prohibited or fly permits were hard to get, such as restricted flying zones, or especially difficult because of climatological and/or topographical conditions.

The first and most important step was to cover the whole area of interest with enough images. The main issues we took into account when taking images from Google Earth or photographing the outcrop in the field using UAVs or tripods were: a) overlapping between pictures and b) minimizing shadowed areas. As a rule of thumb, the more overlapping the better accuracy, but also the longer computing time. Consequently, a compromise was reached between these two factors (Torres-Sánchez et al., 2017). To ensure an appropriate coverage, we took photographs of the outcrops along "scanlines" varying the distance and orientation of the scanlines with respect to the outcrop. Another successful practice was to take several pictures facing different directions from each shooting point.

2.3.2. VOM creation

All the photographs gathered in the field were prepared before creating the VOM.

Regarding the photograph selection, not all the photographs taken were necessary to create the VOM. Thus, some photographs, that were redundant, were discarded to make the computing process faster. Later on, more photographs were added to improve the VOM when the initial result was not satisfactory or blank areas arose.

Regarding the photograph enhancement, we applied photographic filters implemented in the software Adobe Photoshop (https://www.adobe.com/es/products/photoshop.html) to increment the contrast,

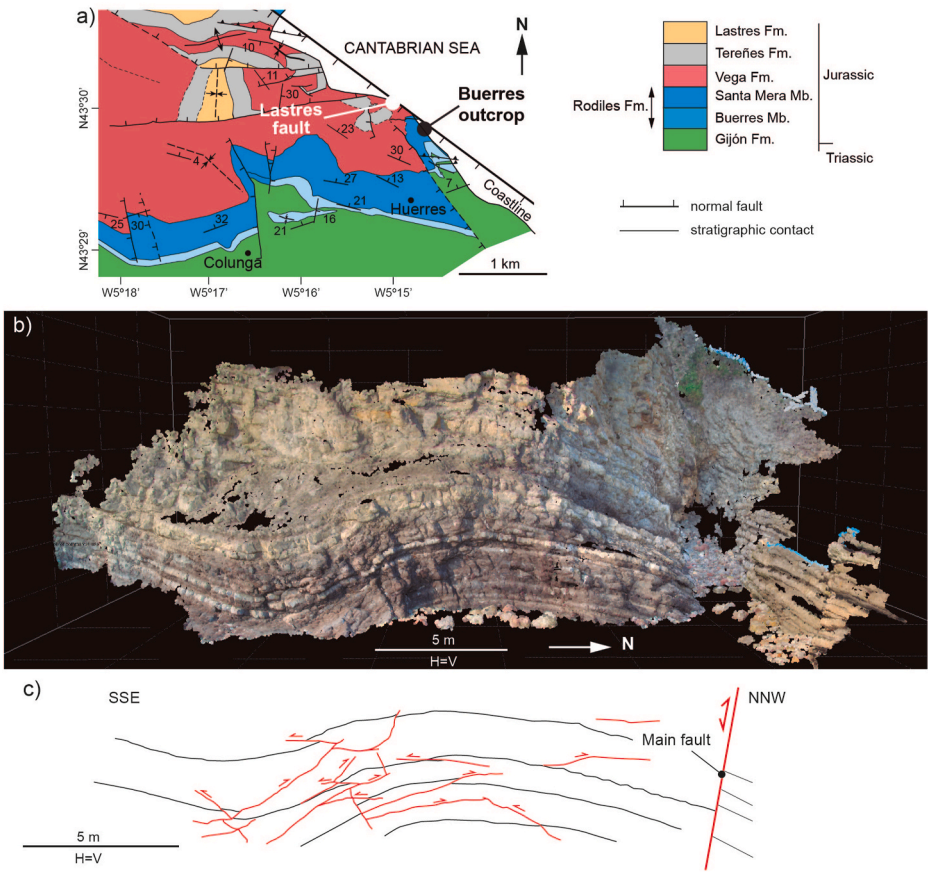

Fig. 8. Buerres outcrop. a) Geological map of the region where the virtual outcrop illustrated in figure b) is located showing the Lastres fault (modified from Uzkeda, 2013), b) point cloud of the outcrop obtained using a photographic camera mounted on a tripod (Uzkeda et al., 2018), and c) geological cross-section obtained from the intersection of 3D geological surfaces with a plane (modified from Uzkeda et al., 2018). See Fig. 1 for location. The latitude and longitude values of an approximately central point within the VOM are 43.4997°N and 5.2429°W respectively. (For interpretation of the references to colour in this figure legend, the reader is referred to the Web version of this article).

brightness, colour balance and/or saturation to improve the photograph quality, homogenize the pictures and to speed up the process. Other techniques, such as High Dynamic Range (HDR) imaging, were used to improve photographs including very lightened areas entwined with shaded zones, which usually happened when the photographs included both outcrop and sky. When the camera was not equipped with HDR as standard, we used the free software Photomatix (https://www.hdrsoft.com) to combine a number of shots for each image (typically between three and five) taken with different shutter values. This was an issue when many pictures were required to create the VOM and also when we used an UAV under windy conditions that affected its stability.

Today there are many personal applications and online applications capable of building 3D models from 2D photographs, some of which work fully automatically. However, we employed an academic license of the software Pix4DMapper (https://www.pix4d.com/product/pix4dmapper-photogrammetry-software) and the free software VisualSfM (http://ccwu.me/vsfm) (Wu, 2013) to create the VOMs using the data collected in the field and pre-processed in the laboratory. Regarding VisualSfM, this software follows the Sfm system developed by Wu et al. (2011) (see Carrivick et al., 2016 for a compendium of some applications of Sfm in Earth Sciences), and sorts out both the intrinsic (camera calibration: calculations of focal length, projection centre and radial distortion) and the extrinsic (resection: determining the camera positions for each photograph) calibrations. To carry out these corrections, the software uses the bundle adjustment method (Triggs et al., 2000; Wu et al., 2011), with automatic detection of matching points using the Scale Invariant Feature Transform (SIFT) algorithm. VisualSfM is also able to load the corresponding parameters and set a fixed calibration if the camera had been calibrated before, which we did for some outcrops. In order to create the point cloud, we ran sparse reconstruction first, so that the bundle adjustment step used multicore bundle adjustment automatically. Subsequently, we carried out a dense reconstruction by using the Patch-based Multi-view Stereo Software (PMVS2) (http://www.di.ens.fr/pmvs/), which is included in the Clustering Views for Multiview Stereo Software package (CMVS) (https://www.di.ens.fr/cmvs/), developed by Y. Furukawa and J. Ponce. This free software grouped the images into manageable packages to make a more exhaustive search, instead of working with all of them at the same time which would be much more expensive from the computational point of view. The package image grouping is based on the previous reconstruction using the bundle adjustment. When working with relatively heavy models we carried out one or more of the following actions: a) down-sample the point cloud for large-scale interpretation when not so much detail was needed using the software Move, b) divide the point cloud into smaller portions to be analysed independently using the software Move, and c) delete areas without interest using initially the software VisualSfm for larger-scale regions and later the software Move for more detailed deleting. From the dense point cloud, the software was also able to generate a triangular textured mesh (Figs. 3a, 4b and 8a). Triangulated textured meshes helped to visualize outcrops, especially when the resulting point clouds were not dense enough. However, in some cases they induced to errors, for instance, when trying to calculate plane orientations by selecting points on the cloud as they simplified the topography or created incorrect connections between the nodes (Höfle et al., 2009; Lindberg et al., 2013; Cawood et al., 2017). Thus, we always saved the original point cloud as a source since interpolated models may lead to wrong results (Otepka et al., 2013).

2.3.3. *VOM georeferencing*

In the case of VOMs derived from UAV's, the images were georeferenced using their internal GPS. Although the x and y coordinates were accurate, some UAV's yielded errors in the z coordinate. These errors were corrected because the altitude of known points in the studied region was available.

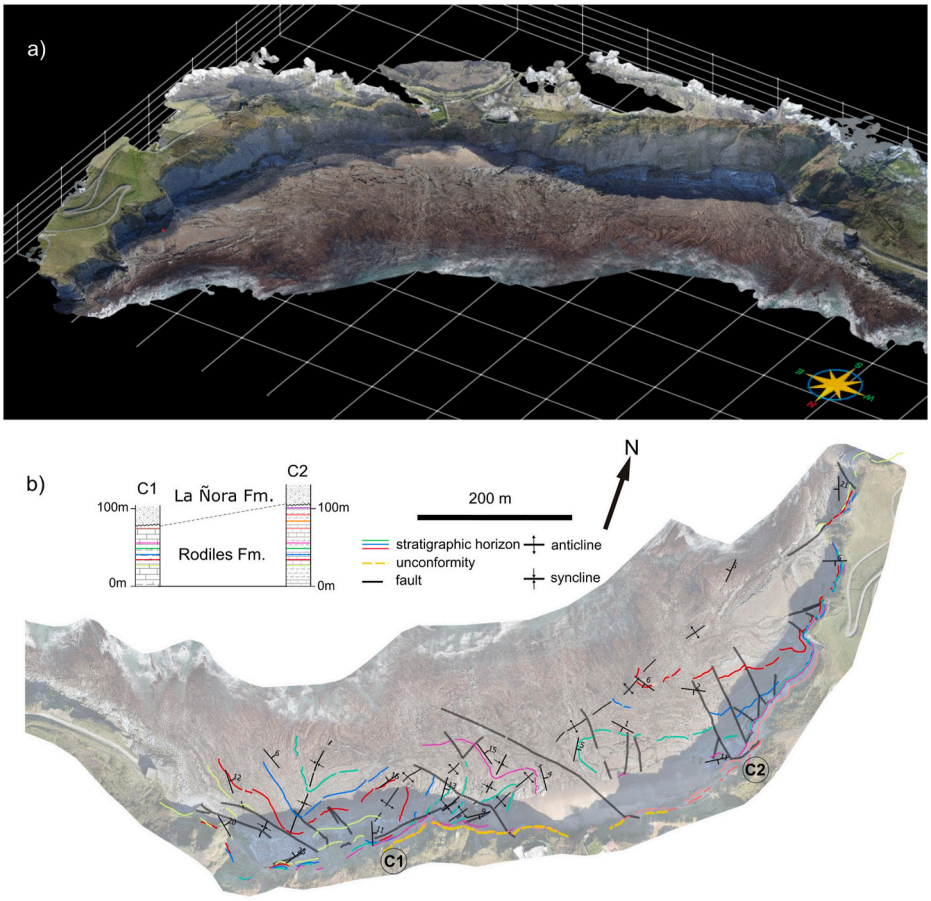

Fig. 9. Peñarrubia outcrop. a) Triangular textured mesh showing the outcrop obtained using a photographic camera mounted on an UAV, and b) geological map derived from the interpretation of a 3D geological model overlapped onto an orthophotograph of the outcrop. See Figs. 1 and 7a for location. The latitude and longitude values of an approximately central point within the VOM are 43.5514° N and 5.6239° W respectively. (For interpretation of the references to colour in this figure legend, the reader is referred to the Web version of this article).

In the case of VOMs constructed using photographic cameras mounted on a tripod, if the camera has an integrated GPS, then the VOM is automatically georeferenced. However, our cameras did not have an integrated GPS. Thus, both the VOMs constructed from photographs taken with cameras in the field and from Google Earth images, required georeferencing to perform quantitative geological analyses because their orientation and size were somewhat arbitrary, i.e., they were not correctly positioned, oriented and scaled. The key issue in this case was the acquisition of georeferenced points in the field and on the Google Earth images that were divided in: a) ground control points (GCP), used to georeference the VOM; and b) check points, left out of the VOM building procedure and employed to assess the accuracy and reliability of the model. Georeferencing a point cloud/mesh requires a minimum of 3 non-linear points, however, in the case of some models that required a lot of detail and/or the mean error was too high, more points were needed (Harwin and Lucieer, 2012; Agüera-Vega et al., 2016; Gindraux et al., 2017; Oniga et al., 2018). The software VisualSfM informed when enough points had been introduced to calculate the required rotation, translation and scaling. Regarding the check points, they were arranged more or less uniformly throughout the whole area of interest and at different depths of view, although zones with less photograph coverage/overlapping were prioritized. Georeferenced points were obtained using a total station and a high precision GPS which were rented for a low cost. A simpler and cheaper solution to acquire georeferenced points consists of using a laser rangefinder, a compass and a laser level (Tavani et al., 2016), however we did not use this solution because it is slightly less accurate. The point-to-point comparison, done manually, was the method employed to assess the accuracy of the resulting VOMs and estimate their error (Fonstad et al., 2013).

In those cases where global coordinates were not necessary, for instance, when the study was focused on a single outcrop and its position with respect to adjacent outcrops was not required, an alternative method was used to extract quantitative information. First of all, we found out surfaces easily identifiable in the field and in the VOM such as bedding, fractures and/or other surfaces. After that, the orientations of these surfaces were measured in the field using a compass and the orientation of the same elements was measured in the "raw" VOM. By calculating the transformation matrix that converts the orientation of the VOM planes into planes with the same orientation than the actual ones and applying it to the point cloud we reorientated the model. To rescale the model, lengths of different elements such as bed thicknesses, fracture spacing and/or distances between other elements were measured in the field using a tape measure and their values compared to the same distances in the VOM to estimate a scale factor to correct the VOM size. In order to obtain good results, we measured dips and strikes of surfaces with different orientations located at different points within the outcrop, and we measured lengths of different magnitudes along different orientations. The reorientation and rescaling of the VOM was carried out using an in-house software but it may be done using the software Move.

2.3.4. *VOM interpretation*

The resulting VOM, either as a point cloud or as a textured triangular mesh, can be interpreted from the geological point of view using a Computer Assisted Virtual Environment (CAVE) and shutting glasses or using a PC/Workstation with optional devices such as virtual reality headsets (Figs. 2c, 3b and 4c, 5c, 6b, 7d, 8c, 9b and 10c). To do so, we employed the in-house software 3D Stereo VDT (Martín et al., 2019) for CAVE, as well as Move and VGRS (http://www.vgeoscience.com) that run in a PC. The abundant tools to draw lines, polygons and points of different colours, to zoom in and out and to rotate the VOMs, and even to carry out measurements such as distances, make all these software

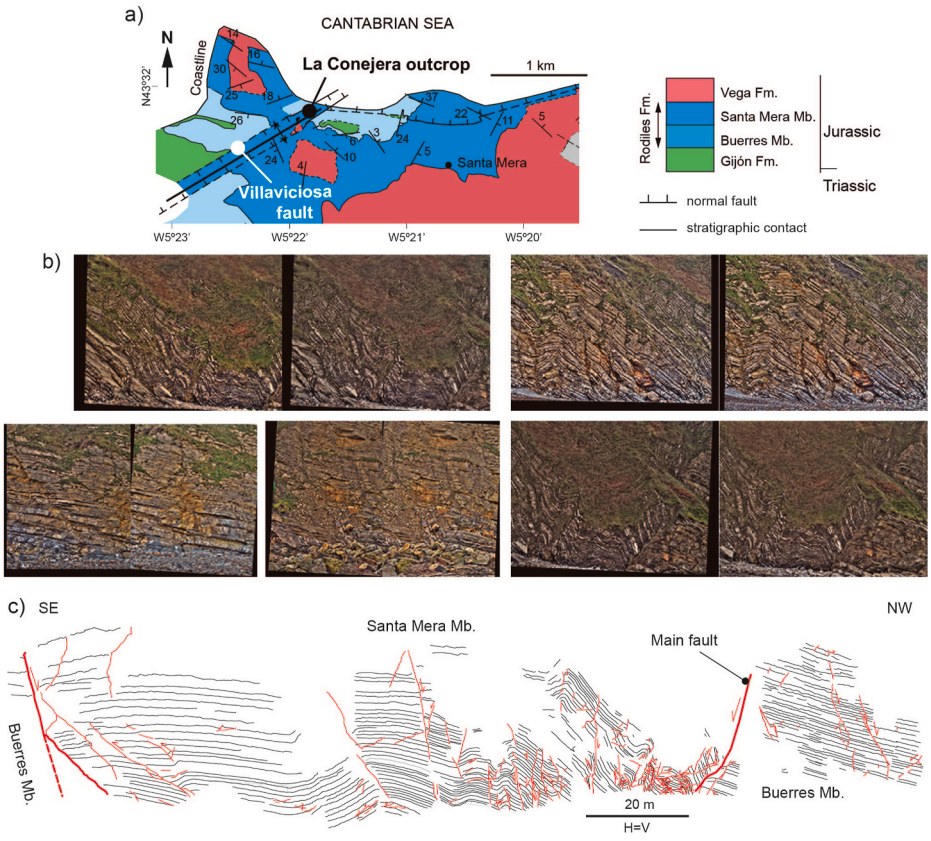

Fig. 10. La Conejera outcrop. a) Geological map of the region where the virtual outcrop illustrated in figure b) is located showing the Villaviciosa fault (modified from Uzkeda, 2013), b) several stereoscopical pairs of photographs of the outcrop obtained using a photographic camera mounted on a tripod, and c) geological cross-section obtained from the projection of the geological interpretation onto two planes (modified from Uzkeda et al., 2013). See Fig. 1 for location. The latitude and longitude values of an approximately central point within the VOM are 43.5324°N and 5.3640°W respectively. (For interpretation of the references to colour in this figure legend, the reader is referred to the Web version of this article).

powerful tools, which allowed us to carry out complete geological interpretations. We first interpreted faults and then horizons in different parts of the outcrop and extended the interpretations until they reached each other to tie the geological interpretation, and we also used data, diagrams and photographs taken in the field to constrain the VOMs interpretation.

2.4. Additional photogrammetric techniques

2.4.1. Orthophotogeological interpretations

From the original photographs taken in the field to construct some of the VOMs and/or from some of the resulting VOMs, we created orthomosaics that were rectified to build orthophotographs (Tavani et al., 2016) with any desired orientation. This was done employing the software Pix4DMapper, which produced good quality orthophotographs (Figs. 3b and 9b).

When the orthophotographs were generated from field photographs, they were interpreted from the geological point of view using drawing packages such as Adobe Illustrator (https://www.adobe.com/es/products/illustrator.html) and the free software Inkscape (https://inkscape.org/es/). This allowed us to obtain orthophotogeological interpretations, i.e., intersections of geological contacts between stratigraphic units, faults, etc. with the topographic surface in which all the elements have the same scale, and therefore, they are free of errors and deformations.

When VOMs interpreted from the geological point of view were available, the process of obtaining orthophotogeological interpretations was carried out as follows. The VOM-derived orthophotographs obtained using Pix4DMapper were scaled, but not georeferenced, except for the zenith orthophotographs that were georeferenced. In the case of orthophotographs not georeferenced, first, we managed to georeference the orthophotographs using the software Move and points of known coordinates. Then the geological interpretations of the VOMs were projected using the same direction employed to construct the orthophotographs and to the same plane using the software Move. Eventually they were overlapped onto the orthophotographs using in-house software to create orthophotogeological interpretations.

2.4.2. Geological interpretation of stereoscopical pairs of photographs

The employment of this technique required five basic steps: a) photograph acquisition, b) control points acquisition, c) intrinsic and extrinsic calibration, d) photograph rectification, and e) geological interpretation.

To photograph the outcrop, we followed some basic rules in order to ensure good quality pictures (Fig. 10b). For instance, we used cameras with fixed-focus lens, whose calibration tends to remain more stable during the whole project and have less optical deformation. Moreover, the pictures were taken with large depths of field to ensure a sharp vision of all the image and, preferably, as HDR images to avoid strong illumination contrasts, i.e., dark and bright areas coexisting. The camera was mounted on a tripod to prevent blurry results. Each stereopair was taken independently, trying to keep the camera looking at the same direction, perpendicular to the outcrop, and moving the camera as parallel as possible to the outcrop face. In general, as it could be expected, the width and height resolutions, i.e., the pixel size of the outcrop, depended on the camera resolution as well as on the distance to the outcrop from the shooting point. The larger the distance, the lower the resolution. The resolution in depth, i.e., parallel to the shooting direction, depended on the two parameters mentioned above, but it was also controlled by the baseline, which is the distance between the two positions of the camera. In general, the larger the displacement, the smaller the uncertainty and, as a consequence, the better the resolution. However, large displacements implied less overlapping between photographs, which meant more stereoscopical pairs of photographs for each area. We tried to find a balance between the voxel size, i.e., the resolution in xyz, and the number of stereoscopical pairs needed.

As is the case of other techniques described above, georeferencing the stereopairs required capturing control points in the field. Theoretically three control points per pair were enough, however, we took about eight points. The reader is referred to a section above to find out how these points were acquired.

Two calibrations were needed to work with stereopairs of photographs: intrinsic and extrinsic. The former consists of getting the actual focal, centre of projection and distortion coefficients of the camera. This required taking a series of photographs from different positions of a rectangular chessboard pattern and loading them in Stereo Rectification, an in-house software based on the OpenCV library (Bradski and Kaehler, 2008). The latter, also called resection, allowed knowing the relative position of the camera at the shooting moments. To do this, the controls points were used in combination with the same in-house software mentioned above. Before interpreting the stereopairs, the images were rectified by reprojecting the image planes of the two camera positions, so that they fell in the exact same plane, i.e., epipolar configuration.

The visualization of the stereo pairs of photographs and their geological interpretation were carried out using Visage, an in-house software for personal computers (Martín et al., 2007) based on the open-source library GLSVe (Martín et al., 2011). This software required the use shutter glasses and allowed drawing polylines to represent different geological elements.

2.5. Deliverables

Different types of information were extracted from the VOMs, orthophotographs and stereoscopical pairs of photographs, which are briefly described below.

2.5.1. Stratigraphic data

In this section we briefly describe different procedures used to obtain stratigraphic data (Fig. 9b) necessary to create the structural models.

First, we selected points on bedding surfaces of different layers from base to top in the VOM and obtained their x, y and z coordinates, using the tools implemented in the software 3D Stereo VDT, Move or VGRS. Then we estimated the dip and strike of the layers in the VOM (the procedure to estimate these values is explained below) or used the values measured in the field. Finally, we calculated orthogonal true thicknesses using a script for Python developed by ourselves or manually. This relatively easy method helped to create stratigraphic logs for inaccessible areas as it only required picking points on the bedding surfaces and estimating their dips. The thickness measurements performed in different parts of the outcrop were compared to decipher whether the stratigraphic thickness was constant or variable.

The orthophotographs were used as auxiliary tools to help establishing stratigraphic correlations from one edge to the other of several outcrops and refine the structural models. Thus, using the software Adobe Photoshop, portions of orthophotographs showing characteristic strata sequences were cropped, moved and overlaid on images from other areas and/or fault blocks to compare both stratigraphic sequences.

2.5.2. Structural data

The different types of measurements from the structural point of view that we carried out are: orientations, number of times an element was repeated and distances. The orientation of planar elements, such as bedding, unconformities, faults and joints, fold limbs and fold axial surfaces, and that of linear elements, such as fold axes and intersection between beds and unconformities, were obtained by identifying points along these elements in the VOMs, obtaining their x, y and z coordinates using the software 3D Stereo VDT, Move or VGRS, and fitting the points to a plane or line employing the software Move (Banerjee and Mitra, 2004; Fernández, 2005 amongst others). A minimum of three points are necessary in the case of planes, while a line can be defined using only two points.

The interpretation of the VOMs also allowed making a fast assessment of parameters such as fracture density as it was relatively simple and quick to draw fractures in the model, draw a scanline across the fractures, count the fractures that intersect the scanline and divide the resulting number by the scanline length.

In addition, measurement of distances such as fault displacement, width of faulted zones, structural relief of a fold and fold wavelength were easily carried out using the tools for length measurements implemented in the software 3D Stereo VDT, Move and VGRS. Alternatively, these measurements were used to evaluate the accuracy and reliability of the VOMs because once these values were obtained, they were manually compared to values measured directly in the field. See Martín et al. (2013, 2019) and Uzkeda et al. (2013, 2018) for further information on structural results obtained from some of the VOMs shown here.

2.5.3. 3D geological models

Once the most important geological elements on a VOM, such as bedding, unconformities, faults and fold axial surfaces were mapped, we built 3D geological models using the software Move. The procedure employed is briefly described below. We usually started by creating the fault framework and work in each fault block independently. Thus, close points belonging to each horizon were fit to a surface and its dip and strike were calculated, and each portion of surface was extended along strike according to the dip and strike calculated. After that, different 3D dip domains (Fernández et al., 2004), in which the dip of the layers was approximately constant, were defined by drawing the axial surfaces corresponding to the boundaries between dip domains. Finally, we interpolated and extrapolated portions of mapped stratigraphic horizons within each dip domain honouring the bedding orientation and the bed thickness. Once the 3D geological model was built, the axial surfaces that bounded the dip domains were erased. We refer the readers to Martín et al. (2019) and Uzkeda et al. (2018) for 3D geological models derived from some of the VOMs shown here.

2.5.4. Geological maps and cross-sections

Other useful results derived from the use of digital techniques are geological maps (Fig. 9b) and cross-sections (Figs. 2c, 4c, 5c, 6b, 7d, 8c and 10c). We used two different ways to generate them briefly described below.

If a 3D geological model had been built, geological maps were constructed by intersecting the interpreted geological surfaces with the topography (Fig. 9b). When outcrops had cantilevers, i.e., overhanging rocks, there were portions of the outcrop that had the same x and y coordinates but different z coordinates. Only those portions of the outcrop closest to the horizontal plane used to construct the map were considered. Geological cross-sections were generated by intersecting the interpreted geological surfaces with a vertical, or inclined plane of a chosen orientation (Figs. 7d and 8c). Both geological maps and cross-sections were easily constructed using the tools implemented in the software Move.

Another option consists of projecting the geological interpretation carried out on a VOM, orthophotograph or stereoscopical pairs of photographs onto a horizontal plane following a vertical direction in the case of geological maps, or onto a vertical or inclined plane following geologically meaningful directions such as fold axes, strikes of beds, etc. in the case of geological cross-sections (Figs. 2c, 4c, 5c, 6b and 10c). In the case of maps, we removed the z coordinate from the lines representing geological features. In the case of cross sections, this operation was carried out using Microsoft Excel spreadsheets (https://www.microsoft.com/en-us/microsoft-365/excel), specific scripts developed for Phyton and the software Move. This procedure consisted of applying a trigonometric formula to the known x, y and z coordinates of each point belonging to each of the interpreted surfaces (bedding, unconformities, fractures, etc.) in order to obtain the new coordinates on the chosen cross section plane.

The second option revealed to be faster, as it does not require to build

surfaces to construct a 3D geological model, and more suitable for essentially "flat" outcrops such as cliff faces or road trenches, while the first method resulted to be more efficient in the case of outcrops with salients and recesses.

3. Geological setting

The virtual outcrops presented here involve carbonate rocks of Devonian and Carboniferous age, and of Jurassic age. The Palaeozoic rocks, affected mainly by folds and thrusts, belong to the Cantabrian Zone, the foreland fold and thrust belt of the Variscan orogen in northwest Iberia developed in Carboniferous times (Fig. 1). This orogen displays an arcuate orocline shape known as Ibero-Armorican or Asturian Arch (Lotze, 1945). The contractional mountain range developed during the Variscan orogeny was dismantled by an erosive episode. After that, a Permian-Triassic rift responsible for normal faults, in some cases resulting from reactivation of previous Variscan structures (Lepvrier and Martínez-García, 1990), propitiated the Asturian basin origin (Fig. 1). The subsequent thermal subsidence event during Late Triassic and Early Jurassic, was followed by an extensional stage that lasted from the end of Early Jurassic until the beginning of Late Jurassic and consisted of development of normal faults, reactivation of previous ones, heating and uplift (Uzkeda et al., 2016). From the Late Jurassic to the lower part of the Early Cretaceous (pre-Barremian) another extensional event caused the reactivation of previous normal faults (Alonso et al., 2018). This episode was related to the rift responsible for the Bay of Biscay opening. From middle Early Cretaceous to Late Cretaceous, a thermal subsidence episode occurred. Convergence between the Iberian and Eurasian tectonic plates during the middle-late part of the Eocene to the beginning of the Miocene (Álvarez-Marrón et al., 1997; Gallastegui, 2000) caused the Alpine orogeny. This contractional event, responsible for the Cantabrian Mountains formation, involved selective reactivation of previous structures, generation of new thrusts and uplift (Lepvrier and Martínez-García, 1990; Pulgar et al., 1999; Alonso et al., 2009; Uzkeda et al., 2016). The structural framework constructed during this contractional event was exhumed during the late part of the Eocene to the beginning of the Oligocene (Fillon et al., 2016), making visible the outcrops in the southern slope of the mountains presented here. During Early Pleistocene or before (Álvarez-Marrón et al., 2008) a narrow coastal strip of Palaeozoic and Mesozoic rocks were eroded, unconformably covered by Quaternary sediments and uplifted above the present-day sea level (e.g., Flor, 1983; Mary, 1983). The emergence of the coastal area, from which various VOMs presented here have been obtained, was accompanied by neotectonic activity such as faulting (e.g., Gutiérrez-Claverol et al., 2006; Álvarez-Marrón et al., 2008) and small magnitude earthquakes (e.g., López-Fernández et al., 2004).

4. North-Northwest Iberia VOMs

4.1. Cantabrian Zone

The Cantabrian Zone is the foreland fold-and-thrust belt of the Northwest-Iberia Variscan Orogen developed during Carboniferous times (Lotze, 1945; Julivert et al., 1972) (Fig. 1). The Cantabrian Zone involves a Palaeozoic stratigraphic succession from Cambrian to Carboniferous, made up of both siliciclastic (slates, sandstones and microconglomerates) and carbonate (marls, limestones and dolomites) sedimentary rocks with sporadic coal beds and volcanic rocks. This zone developed under diagenetic conditions although some localities reached very low or low-grade metamorphism. It is a typical thin-skinned belt, constituted by different types of thrust systems and folds, where tectonic foliations are lacking except for small areas (e.g., Julivert, 1971, 1983; Savage, 1979, 1981; Pérez-Estaún et al., 1988; Pérez-Estaún and Bastida, 1990; Aller et al., 2004). In cross section, the Cantabrian Zone exhibits a wedge geometry thinning eastwards, i.e., towards the foreland. In map view, it displays a curved trend around an approximately E–W axial surface with the core to the east, known as Ibero-Armorican or Asturian Arc.

4.1.1. Cacabillo

The Cacabillo outcrop is located in the almost inaccessible slope of a valley near the Cacabillo village, in the southwestern portion of the Cantabrian Zone close to the core of the Ibero-Armorican or Asturian Arc, where NW–SE trending structures predominate (Fig. 1). The outcrop is located in the hinge zone of the several kilometres long Cacabillo anticline (Navarro-Vázquez and Rodríguez-Fernández, 1978), also known as Puerto de Somiedo anticline (Bastida et al., 1984) (Fig. 2a). This anticline is a NW–SE trending, tight fold with a subvertical axial surface. A subvertical, NW–SE trending fault of small displacement in the core of the Cacabillo/Puerto de Somiedo anticline separates the southwest limb from the hinge and the northeast limb. This anticline, mapped in Navarro-Vázquez and Rodríguez-Fernández (1978), Bastida et al. (1984), Alonso et al. (1989) and Merino-Tomé et al. (2014), involves an Ordovician-Carboniferous succession (Fig. 2a) and was developed during the Variscan orogeny.

A VOM was created using georeferenced Google Earth images (Fig. 2b), and an undistorted geological cross-section was constructed by projecting the geological interpretation of the VOM onto a selected plane (Fig. 2c). Below is a description of the outcrop derived from the VOM geological interpretation and from the cross section.

The rocks shown in the virtual outcrop belong to two Devonian stratigraphic units according to the available geological maps and sections (Navarro-Vázquez et al., 1982). The upper unit, the Santa Lucía Fm., is a limestone unit with sparse marls and slates, whereas the lower unit, La Vid Gr., is mainly made up of dolostones, slates, limestones and marls. The grey layers that stand out in the relief correspond to the limestones of the Santa Lucia Fm., while the lower regions where layers are hardly recognized correspond to La Vid Gr. (Fig. 2b and c). The outcrop consists of a fold train formed by two anticlines and two synclines whose dimensions reach hundreds of meters. The limbs of each fold dip towards opposite senses and the axial surfaces are subvertical. Several planar faults, whose displacement can reach a hundred meters, cut and offset the folds; in particular, they are well developed in the southwest limbs of the folds and dip in opposite sense to that of the limbs. Folded thrusts, responsible for the repetition of some beds within the Santa Lucia Fm., have also been identified. These thrusts develop flats in most of their trajectory, although some ramps are recognized, especially near the hinge of the anticline located to the northeast. These folds and faults are second-order structures developed in the hinge of the larger-scale Cacabillo/Puerto de Somiedo anticline, which contribute to its thickening. We refer the reader to Martín et al. (2019) for more information on the features of this virtual outcrop.

4.1.2. Las Palomas

This outcrop, located on the steep slope of a local road near Las Palomas bridge, belongs to the southwestern portion of the Cantabrian Zone close to the Ibero-Armorican or Asturian Arc core, where NW–SE trending structures are common (Fig. 1). The outcrop is located in the southwest limb of the kilometre-scale Vega de Los Viejos syncline (Navarro-Vázquez et al., 1982), a tight, NW-SE trending syncline whose axial surface is subvertical (Fig. 2a). This large syncline, developed during the Variscan orogeny, involves an Ordovician-Carboniferous succession, and its southwestern limb is unconformable covered by Uppermost Carboniferous deposits as shown in the geological maps and sections by Navarro-Vázquez and Rodríguez-Fernández (1978), Bastida et al. (1984), Alonso et al. (1989) and Merino-Tomé et al. (2014) (Fig. 2a).

A VOM was created from pictures taken in the field with a photographic camera mounted on a tripod (Fig. 3a). Subsequently, an orthophotograph derived from the VOM was geologically interpreted in order to obtain a geological cross section (Fig. 3c). A description of the outcrop, based on the visualization and geological interpretation of the

VOM, orthophotograph and cross section, is presented in the next paragraph.

The rocks displayed in the virtual outcrop are limestones that belong to the Barcaliente Fm. of Carboniferous age according to Navarro-Vázquez et al. (1982) (Fig. 3a and b). The outcrop is formed by a train of metre-scale folds. In general, the axial surfaces of the folds dip steeply to the NE and the limbs of most folds dip towards opposite directions. There is a thick, competent limestone layer the middle part of the stratigraphic succession. Below this layer, the limestones are thinly bedded, while above it they have an intermediate thickness in between that of the thinly bedded layers and that of the thick layer. This competent layer behaves differently from the over- and underlying layers and in turn it is the boundary between mechanically different behaviours. Thus, this layer gives rise to a box syncline and a box anticline in the central part of the outcrop. The beds above this limestone layer exhibit hinge collapses in the anticline illustrated on the left side of the image, while the beds below this limestone layer are folded by many minor folds on the right side of the image. The anticlines and synclines illustrated in this VOM are second-order folds that have contributed to thicken the southwest limb of the larger-scale Vega de Los Viejos syncline. The syncline shown in the central part of the outcrop has been described in Poblet et al. (2022).

4.1.3. San Emiliano

This outcrop is located on the steep slope of a road near the San Emiliano village, in the southwest portion of the Cantabrian Zone and in the southern branch of the Ibero-Armorican Arc, where E-W trending structures dominate (Fig. 1). The outcrop is located in the north limb of the kilometre-scale Huergas-Valgrande anticline (Marcos, 1968), also known as Villasecino anticline (De Sitter and Van den Bosch, 1969) (Fig. 4a). This anticline is a tight and approximately upright fold that strikes E–W. A subvertical, E-W trending fault runs along the core of the anticline. This regional-scale anticline, interpreted as a Variscan fold that involves a Cambrian to Carboniferous stratigraphic succession, has been displayed in several geological maps and cross sections (De Sitter, 1962; Marcos, 1968; Martínez-Álvarez et al., 1968; Alonso et al., 1989; Suárez-Rodríguez et al., 1991; Merino-Tomé et al., 2014) (Fig. 4a).

A VOM was created using a photographic camera mounted on a tripod (Fig. 4b), and a cross section was obtained from the projection of the VOM geological interpretation onto a selected plane (Fig. 4c). The description of the outcrop below comes from the visualization and geological interpretation of the VOM and the cross section.

The rocks shown in the virtual outcrop belong to the Carboniferous Alba (or Genicera) Fm., colloquially known as “Carboniferous griotte limestone”, according to the available geological maps (Rodríguez-Fernández et al., 1991) (Fig. 4b and c). In outline, this outcrop consists of a homoclinal set of layers that dip steeply to the NNW. Taking into account the behaviour of the layers regarding deformation, they may be divided into three mechanical units. The lower mechanical unit, located to the south-southeast, is mainly made up of red limestones (“griotte” facies) affected by large folds and faults, and the faults dip steeply. The intermediate mechanical unit, located in the central part of the outcrop, is formed by alternations of radiolarites and slates, and both folds and faults are more abundant than in the lower unit, they are smaller, and the faults display a wide range of dips. In the upper mechanical unit, located to the north-northwest and constituted by grey limestones with some reddish shale interbeds, the faults are scarce. According to Masini et al. (2010a) this outcrop was tilted in a counter clockwise sense around an ENE-WSW subhorizontal axis. The structures make sense from the geological point of view when removing this rotation until the layers reach a sub-horizontal position. Thus, the lower mechanical unit corresponds to a thrust ramp anticline located in the hangingwall of a series of thrusts that dip to the N in the rotated image. This lower unit is detached from the underlying units (south-southeast main fault in Fig. 4c). A detachment located at the top of the lower unit separates this unit from the intermediate unit (central main fault in Fig. 4c). The intermediate mechanical unit displays several detachment folds with abundant minor thrusts. Another detachment separates the intermediate from the upper unit. The upper mechanical unit is almost undeformed. These structures are responsible for thickening the north limb of the larger-scale Huergas-Valgrande/Villasecino anticline. This virtual outcrop is presented here for the very first time, however, the reader can consult Masini et al. (2010b) and Bulnes et al. (2019) for further information on this outcrop.

4.1.4. La Ballota

This outcrop is a coastal cliff located in La Ballota Beach, in the northeastern part of the Cantabrian Zone and in the north branch of the Ibero-Armorican or Asturian Arc, where E–W trending structures are the most common ones (Fig. 1). La Ballota outcrop is only accessible during periods of low tide. The outcrop is located in the north limb of a hundred-metres long anticline located to the north of the Cue anticline (Fig. 5a). This anticline is a tight, E-W striking fold, whose axial surface dips steeply to the N. This anticline is interpreted as a ramp fold located in the hangingwall of an E–W, S-directed thrust that dips steeply to the N. This anticline is supposed to be a Variscan structure that involves an Ordovician, Devonian and Carboniferous succession according to the geological maps and sections constructed by Martínez-Álvarez (1965), Martínez-García (1980), Marquínez (1989), Merino-Tomé et al. (2014), De Ana (2015) and Bulnes et al. (2016) (Fig. 5a).

A VOM was constructed using a photographic camera mounted on a tripod (Fig. 5b), and a cross section was obtained from the projection of the geological interpretation onto a selected plane (Fig. 5c). The main features of the outcrop are described below based on the geological interpretation of the VOM and on the cross section.

According to Martínez-García et al. (1981) this outcrop is composed of limestones with slates that belong to the Carboniferous Alba Fm., also known as Genicera Fm. (Fig. 5b and c). This outcrop includes a very tight anticline in the north-northwest part and a closed syncline that occupies the central and south-southeast part of the outcrop. The hinge of the anticline shows extraordinary thickening at some incompetent stratigraphic levels. Both folds are a few metres wide and tall, and their axial surfaces are subvertical. The layers are cut and offset by abundant metre-scale, SSE directed thrusts whose dip varies from horizontal to subvertical since they are folded by the anticline and the syncline. In most of the trajectory of these thrusts, hangingwall flats over footwall flats occur, although some hangingwall and footwall ramps occur as well, specially near the anticline hinge and towards the south-southeast portion of the outcrop. Thus, this outcrop is basically a stack of folded thrust sheets. The axial surface of the folds, and in particular that of the syncline, do not exhibit a rectilinear path in cross-sectional view from the upper layers to the lower ones, but display “jumps” from one thrust sheet to the underlying one. The reason is that bedding surfaces were not parallel before folding because they had been cut and offset by thrusts. All these structures contributed to thicken the north limb of the larger-scale anticline located to the north of the Cue anticline.

4.1.5. Andrín

This outcrop is a coastal cliff located in the Andrín Beach, in the northeastern part of the Cantabrian Zone and in the north branch of the Ibero-Armorican or Asturian Arc, where the structures trend E–W (Fig. 1). The outcrop can only be visited during low tide periods. The outcrop belongs to the north limb (backlimb) of the kilometre-scale Cue anticline (Martínez-García et al., 1981), a closed, E–W striking fold, whose axial surface dips steeply to the N (Fig. 5a). The Cue anticline is interpreted as a ramp fold located in the hangingwall of an E–W thrust that dips steeply to the N and whose hangingwall exhibits a southwards sense of motion. The Cue anticline, developed during the Variscan orogeny, involves an Ordovician, Devonian and Carboniferous succession as shown in the available geological maps and sections (Martínez-Álvarez, 1965; Martínez-García, 1980; Marquínez, 1989; Merino-Tomé et al., 2014; De Ana, 2015; Bulnes et al., 2016) (Fig. 5a).

A VOM was constructed using a photographic camera mounted on a tripod (Fig. 6a) and its geological interpretation was projected onto a selected plane to construct an undistorted geological cross-section (Fig. 6b). An outcrop description derived from the VOM interpretation and from the geological cross-section is presented below.

The studied virtual outcrop consists of red limestones that belong to the Carboniferous Alba (or Genicera) Fm. according to the available geological maps (Martínez-García et al., 1981) (Fig. 6a and b). In the southeastern part of the outcrop, several metre-scale, tight anticlines and synclines, whose hinges exhibit thickening with respect to the limbs and whose limbs dip to the same direction, appear. The axial surfaces of these folds are curve; thus, they dip moderately upsection but progressively become gently dipping to the SE until they are subhorizontal downsection because they have subsequently been refolded by another set of folds, giving rise to type 3 fold interference patterns (Ramsay, 1967). All these structures are located in the hangingwall of a decametre-scale, NW-directed reverse fault that dips steeply to the S and appears in the central part of the outcrop. In the footwall of this fault, i.e., in the northwestern part of the outcrop, a large syncline and a smaller anticline with thickened hinges, NW-dipping limbs and SW-dipping axial surfaces crop out. This virtual outcrop was presented in Martín et al. (2019), however, its structural features are described here for the very first time.

4.2. Asturian Basin

The Asturian Basin is an inverted extensional basin that crops out along the North Iberian Margin and extends northwards under the Cantabrian Sea (Fig. 1). This basin is filled in with a Permian-Triassic siliciclastic succession including some volcanoclastic, carbonate and evaporitic deposits, a Lower-Middle Jurassic succession composed of marls and limestones, an Upper Jurassic succession formed by marls, shales and sandstones with some limestones, and Cretaceous alternations of siliciclastic and carbonate rocks (García-Ramos and Gutiérrez-Claverol, 1995). The two most important angular unconformities within the basin are located in between the Permian-Triassic succession and the Variscan basement of the Cantabrian Zone, and between the Lower Jurassic marine successions and the continental/transitional Upper Jurassic rocks (Valenzuela et al., 1986). The internal structure of the basin mainly consists of Mesozoic normal faults of different orientations, some of them reactivated as reverse, oblique or strike-slip faults during a Cenozoic contractional episode, responsible for different modes of inversion tectonics from pure fault reactivation to buttressing structures (e.g., Lepvrier and Martínez-García, 1990; Uzkeda et al., 2016).

4.2.1. Cervigón

This outcrop is a small part of a coastal cliff located in the Peñarrubia Beach, near the Cervigón viewpoint, in the north-northwest part of the emerged portion of the Asturian Basin (Fig. 1). Stones may fall from the top of the high cliff where the outcrop is located and the outcrop can only be visited during low tide periods. According to the available geological maps, the outcrop is located in the southwest limb of a kilometre-scale, very open syncline whose trend is NW-SE and involves a Jurassic succession (Fig. 7a and b). The portion of the basin where this outcrop is located was mapped in Beroiz et al. (1972b), Suárez-Vega (1974), Gutiérrez-Claverol et al. (2002), Merino-Tomé et al. (2014) and Odriozola (2016).

The VOM constructed using images taken with a photographic camera mounted on a tripod (Fig. 7c) was the basis for a 3D geological model. A geological cross-section was obtained from the intersection of 3D geological surfaces with a selected plane (Fig. 7d). An outcrop description, derived from the geological interpretation of the VOM, and from the 3D model and geological cross-section, is presented below.

The studied virtual outcrop consists of marls and limestones that belong to the Rodiles Fm. of lower Early Jurassic age in this region (Suárez-Vega, 1974) (Fig. 7c and d). The most striking structures in this outcrop are a metre-scale monoclinal anticline and a monoclinal syncline; these open folds are asymmetric and their axial surfaces dip moderately to the E. Two metre-scale, W-directed reverse faults with small displacement are developed in the hinge zone of the folds. The asymmetry of the folds, the sense of motion of the reverse faults and the cross-cutting relationships with other structures, which will be discussed below, suggest that these folds and faults have a genetic relationship. The tip of the lower reverse fault ends up against the syncline axial surface, while the other reverse fault involves upper stratigraphic horizons, runs through the common limb between the two folds and ends upsection as a hangingwall flat over a footwall flat. This suggests that the structure could be a fault-propagation fold related to the lower fault, while the other reverse fault would correspond to a breakthrough fault. An E-directed detachment, folded and offset by a reverse fault, occurs in the middle part of the stratigraphic succession. This detachment, in turn, cuts and offsets a metre-scale, E-directed normal fault with small displacement located in between the anticline and syncline hinges. The outcrop also includes a series of subvertical strike-slip faults; although these faults cut and offset the detachment, their temporal relationship with the folds, and the reverse and normal faults, are difficult to define since they develop in regions where the layers are flat-lying. Thus, apart from the strike-slip faults, the chronology of the structures would start with a normal fault, followed by a detachment, and finally the folds and reverse faults. The geometry of these structures suggests that the whole structure resulted from positive inversion tectonics so that the anticline hinge would nucleate in the normal fault hangingwall while the syncline in the footwall. The reader is referred to Uzkeda et al. (2018) for more information regarding this virtual outcrop.

4.2.2. Buerres

This outcrop is a coastal cliff located near the Huerres village, also called Buerres, in the north-northeast portion of the emerged portion of the Asturian Basin (Fig. 1). The cliff where the outcrop is located is high, so that stones can fall, and the outcrop can only be visited during low tide periods. The studied outcrop is located in the downthrown block of the Lastres fault, very close to the fault surface (Fig. 8a). This kilometre-scale, normal fault exhibits a NW-SE strike, dips steeply to the SW and involves Jurassic rocks (Uzkeda, 2013). The region around the studied outcrop was mapped by Beroiz et al. (1972a), Suárez-Vega (1974), Merino-Tomé et al. (2014) and Uzkeda et al. (2016) (Fig. 8a).

A VOM was obtained using a photographic camera mounted on a tripod (Fig. 8b). Its geological interpretation was used to construct a 3D geological model and the intersection of 3D geological surfaces with a plane allowed us to construct a geological cross-section (Fig. 8c). Below is a description of the outcrop derived from the visualization and geological interpretation of the VOM and from the geological cross-section.

The virtual outcrop analysed here involves marls and limestones that belong to the Rodiles Fm., whose age in this region ranges from Early to Middle Jurassic (Suárez-Vega, 1974) (Fig. 8b and c). One of the most important structures in this outcrop is a metre-scale, SSE-directed fault, that currently exhibits normal motion, dips steeply to the SSE, and is located in the north-northwest edge of the outcrop. In the fault hangingwall, the layers are affected by a metre-scale, smooth anticline-syncline pair. The axial surfaces of these folds are subvertical, but the folds are slightly asymmetric since the south-southeast limb of the anticline is somewhat shorter and its dip is steeper than that of the north-northwest limb. The folded layers are cut and offset by a set of metre-scale, reverse faults with small displacements and gently dips to both the SSE and the NNW. They are thrusts and backthrusts. The cross-cutting relationships between the SSE-dipping and the NNW-dipping thrusts are complex, as some SSE-dipping thrusts cut and offset some NNW-dipping thrusts, but the opposite situation also occurs. This indicates that thrusts and backthrusts are approximately synchronous. Both the anticline-syncline pair and the thrusts and backthrusts are probably simultaneous structures. Since all these structures are only

developed in the hangingwall of the normal fault very close to it, they are interpreted as buttressing structures. This hypothesis is corroborated by the fact that the hangingwall succession includes more marls and shales than that in the fault footwall, i.e., the hangingwall rocks are less competent than the footwall ones. Thus, the initially normal fault was responsible for a buttressing effect and was reactivated as a reverse fault giving rise to a positive tectonic inversion structure. The reader is addressed to Uzkeda et al. (2018) for further information on this virtual outcrop.

4.2.3. Peñarrubia

This outcrop covers part of the coastal cliff, part of the beach and part of the platform located in the Peñarrubia Beach, in the north-northwest part of the emerged portion of the Asturian Basin (Fig. 1). Stones may fall from the upper parts of the high cliff and the platform can only be accessed during low tide periods. The outcrop comprises the hinge zone and both limbs of a kilometre-scale, NW-SE trending syncline. This smooth fold involves a Jurassic succession (Fig. 7a). Several geological maps illustrate the portion of the basin where this outcrop is located (Beroiz et al., 1972b; Suárez-Vega, 1974; Gutiérrez-Claverol et al., 2002; Merino-Tomé et al., 2014; Odriozola, 2016).

A VOM created using a photographic camera mounted on an UAV (Fig. 9a) was used to construct a 3D geological model. A geological map was obtained from the interpretation of the 3D geological model overlapped onto an orthophotograph of the outcrop (Fig. 9b). The geological description presented below is derived from the VOM geological interpretation, as well as from the 3D geological model and the geological map.

This virtual outcrop is made up of alternations of marls and limestones that belong to the Rodiles Fm., which in this region has a lower Early Jurassic age, as well as of conglomerates, sandstones and shales of La Ñora Fm., whose age is Upper Jurassic according to Suárez-Vega (1974) (Fig. 9a and b). From a stratigraphic point of view, the map clearly shows an angular unconformity in between La Ñora Fm. and the Rodiles Fm., so that in the southwestern part of the outcrop La Ñora Fm. lays on older Rodiles Fm. beds (stratigraphic log C1 in Fig. 9b) than in the northeast part of the outcrop (stratigraphic log C2 in Fig. 9b). Regarding the structure, several NE-SW trending anticlines and synclines of hectometre lengths are recognized. Various faults have been also mapped. Most of these faults strike from ENE-WSW to NE-SW, reach a few hundred meters length, and cut and offset the traces of the aforementioned folds pointing out that they are younger.

4.2.4. La Conejera

This outcrop is a coastal cliff located in La Conejera Inlet, in the north-northeast part of the emerged portion of the Asturian Basin (Fig. 1). Stones may fall from the high cliff where the outcrop is located and part of the outcrop can only be visited during low tide periods. According to Uzkeda et al. (2013), this outcrop is supposed to show part of the kilometre-scale Villaviciosa fault (Fig. 10a). This fault is a NE-SW striking structure with vertical or steep dip to the SE that involves Mesozoic rocks in both fault blocks. The outcrop and surrounding regions were mapped by Pignatelli et al. (1972), Suárez-Vega (1974), Merino-Tomé et al. (2014), Uzkeda et al. (2016) and Granado et al. (2018) (Fig. 10a).

Stereoscopical pairs of photographs of the outcrop were obtained using a photographic camera mounted on a tripod (Fig. 10b), and a geological cross-section was obtained from the projection of the geological interpretation onto two selected planes (Fig. 10c). We describe the outcrop below according to our geological interpretation of the stereoscopical pairs and to the geological cross-section.

The marls and limestones that make up the studied virtual outcrop belong to the Rodiles Fm., with an age of Early Jurassic in this area (Suárez-Vega, 1974) (Fig. 10b and c). Two are the most important structures in this outcrop and both are located in the centre-northwest part of the outcrop. The first structure is a decametre-scale, normal fault that dips steeply to the SE and causes a notable layer displacement. The second one is a decametre-scale, open monoclinal anticline, whose southeast limb is subhorizontal whereas its northwest limb dips moderately to the NW against the fault mentioned above. The geometry of this monocline and its development in the hangingwall of the mentioned fault suggest that it could be interpreted as a rollover anticline related to the normal fault motion. On a metre-scale, there are abundant normal and reverse faults as well as folds. Reverse faults and folds postdate normal faults, are only developed in the hangingwall of the main fault and their density increases from the southeast towards the mentioned fault, while the interlimb angle of the folds decreases from the southeast towards the mentioned fault. The variation in the characteristics of these smaller-scale structures and their structural position suggest that they resulted from a buttressing phenomenon against the main normal fault causing its reactivation as a reverse fault. The fact that the rocks located in the footwall of the normal fault exhibit higher limestone and lesser marl contents than those located in the hangingwall is in agreement with this hypothesis. Thus, the overall structure of this outcrop resulted from positive inversion tectonics. We refer the reader to Uzkeda et al. (2013) for further information about the features of this virtual outcrop.

5. Final considerations

There is no doubt that the application of digital techniques to the study of natural geological structures is a significant advance in Structural Geology, facilitating the process of collecting and processing field data and, in some situations, supplying additional information that would have been hard to obtain using traditional techniques solely. Once the images of the structures, their geological interpretation, as well as additional data, are “inside” our computer, a world of possibilities opens up to extract the information as geological maps and sections in any direction of space, as well as 3D geological models, which makes understanding them much faster and easier.

Given their benefits, we encourage all the structural geologists to use digital techniques and create more VOMs all over the world. In this sense, this work might help all those structural geologists who would like to use digital techniques to construct 3D geological models, geological cross-sections and maps, and obtain additional structural data, from outcrops of natural structures.

All the north-northwest Iberia outcrops studied here involve steep slopes (valley slopes, road slopes, coastal cliffs). On the one hand, the analysis of the VOMs has allowed obtaining dips, strikes and dip directions of layers, unconformities, faults, joints, fold limbs, fold axial surfaces, fold axes and intersection lines between beds and unconformities, located in the inaccessible parts of the outcrops. On the other hand, outcrops such as Cacabillo, La Ballota, Andrín, Cervigón and La Conejera exhibit abundant inlets and outlets that make it difficult to correctly visualize and graphically represent the structures. However, the construction of VOMs has made it possible to visualize the 3D structural complexity and project the interpretations onto undistorted 2D geological sections, which has greatly facilitated their understanding. In the case of large outcrops such as Cacabillo, Peñarrubia and La Conejera, the geological interpretation of the VOMs has permitted establishing local stratigraphic columns at outcrop scale, which has allowed the layers to be correlated from one edge to the other edge of the outcrop, and hence better understand the structures that affect them.

The most obvious use of the VOMs of the north-northwest Iberian Peninsula presented here is related to research and involves deciphering their main structural features. However, they also represent a contribution as a virtual fieldtrip across this part of the world, and are interesting from the teaching point of view as well, especially if they are incorporated into platforms specifically designed for these purposes, such as 3DGaia (https://www.imagedreality.com/3d-gaia-vr-app). Regarding virtual fieldtrips and teaching, these VOMs could help Earth Science professionals and students to figure out the structural styles of

the Cantabrian Zone and the Asturian Basin, as well as to learn about contractional and inversion tectonics structures. Thus, they can remotely visualize the VOMs from different perspectives, interpret them and understand these outcrops located in regions of difficult access (steep slopes, cliffs by the sea, intertidal regions) at any time, but specially during times when carrying out fieldwork is not possible because of travel restrictions caused by pandemics or similar situations. In addition, these VOMs allow costs to be reduced because the virtual fieldtrips can be repeated as many times as desired and involve less travel, which in turn reduces the carbon footprint, while increasing the visibility of the geology of this part of the world as well as equality, since the outcrops are accessible to people with disabilities.

The digital techniques have led to a sort of "revolution" within the Structural Geology, that advances day by day, and to which we should be aware, however, we believe we must continue combining both traditional and digital techniques because we found all of them useful and complimentary.

Credit author statement

Hodei Uzkeda: Conceptualization, Methodology, Software, Validation, Investigation, Writing – original draft, Writing – review & editing, Visualization. Josep Poblet: Conceptualization, Validation, Investigation, Resources, Writing – review & editing, Supervision, Project administration, Funding acquisition. Marta Magán: Methodology, Software, Validation, Investigation, Writing – review & editing, Visualization. Mayte Bulnes: Validation, Investigation, Resources, Visualization, Supervision, Project administration, Funding acquisition. Santiago Martín: Methodology, Software, Validation, Resources. David Fernández-Martínez: Methodology, Investigation

Declaration of competing interest

The authors declare that they have no known competing financial interests or personal relationships that could have appeared to influence the work reported in this paper.

Acknowledgments

This study was supported by research projects CN-16-014, CN-16-015 and CN-16-016 funded by the oil company Repsol. We are grateful to C. Wu for permission to use the software VisualSfM. We thank the editors of this special issue Virginia Toy, Clare Bond, Sandra McLaren and Nic Barthla for the opportunity to present our work in this volume. Comments by C. Connors and P. Granado substantially improved the manuscript.

References

Agüera-Vega, F., Carvajal-Ramírez, F., Martínez-Carricondo, P., 2016. Accuracy of digital surface models and orthophotos derived from unmanned aerial vehicle photogrammetry. J. Survey Eng. 143 (2), 04016025.

Aller, J., Álvarez-Marrón, J., Bastida, F., Bulnes, M., Heredia, N., Marcos, A., Pérez-Estaún, A., Pulgar, J.A., Rodríguez-Fernández, R., 2004. Estructura, deformación y metamorfismo (Zona Cantábrica). In: Vera, J.A. (Ed.), Geología de España. Sociedad Geológica de España-Instituto Geológico y Minero de España, Madrid, pp. 42–49.

Allmendinger, R.W., Siron, C.R., Scott, C.P., 2017. Structural data collection with mobile devices: accuracy, redundancy, and best practices. J. Struct. Geol. 102, 98–112.

Alonso, J.L., Álvarez-Marrón, J., Pulgar, J.A., 1989. Síntesis cartográfica de la parte sudoccidental de la Zona Cantábrica. Trab. Geol. 18, 145–155.

Alonso, J.L., Barrón, E., González Fernández, B., Menéndez Casares, E., García-Ramos, J. C., 2018. Extensión e inversión tectónica alpinas en el área de Sariego. Control ejercido por la estructura varisca subyacente (Asturias, norte de España). Trab. Geol. 36, 45–60.

Alonso, J.L., Gallastegui, J., García-Ramos, J.C., Poblet, J., 2009. Estructuras mesozoicas y cenozoicas relacionadas con la apertura y cierre parcial del Golfo de Vizcaya (Zona Cantábrica–Asturias). In: Guía de campo del "6° Simposio sobre el Margen Ibérico", vol. 18. Oviedo.

Alonso, J., Pulgar, J., García-Ramos, J., Barba, P., 1996. W5 tertiary basins and Alpine tectonics in the Cantabrian mountains (NW Spain). In: Friend, P., Dabrio, C. (Eds.), Tertiary Basins of Spain: the Stratigraphic Record of Crustal Kinematics. Cambridge University Press, pp. 214–227.

Álvarez-Marrón, J., Hetzel, R., Niedermann, S., Menéndez, R., Marquínez, J., 2008. Origin, structure and exposure history of a wave-cut platform more than 1 Ma in age at the coast of northern Spain: a multiple cosmogenic nuclide approach. Geomorphology 93 (3–4), 316–334.

Álvarez-Marrón, J., Rubio, E., Torné, M., 1997. Subduction-related structures in the North Iberian margin. J. Geophys. Res. Solid Earth 102 (B10), 22497–22511.

Banerjee, S., Mitra, S., 2004. Remote surface mapping using orthophotos and geologic maps draped over digital elevation models: application the Sheep Mountain anticline, Wyoming. AAPG (Am. Assoc. Pet. Geol.) Bull. 88 (9), 1227–1237.

Bastida, F., Marcos, A., Pérez-Estaún, A., Pulgar, J.A., 1984. Geometría y evolución estructural del Manto de Somiedo (Zona Cantábrica, NO de España). Bol. Geol. Min. 95 (6), 3–25.

Bellian, J.A., Kerans, C., Jennette, D.C., 2005. Digital outcrop models: applications of terrestrial scanning lidar technology in stratigraphic modeling. J. Sediment. Res. 75 (2), 166–176.

Bemis, S.P., Micklethwaite, S., Turner, D., James, M.R., Akciz, S., Thiele, S.T., Bangash, H.A., 2014. Ground-based and UAV-based photogrammetry: a multi-scale, high-resolution mapping tool for structural geology and paleoseismology. J. Struct. Geol. 69, 163–178.

Berger, Z., Lee Williams, T.H., Anderson, D.W., 1992. Geologic stereo mapping of geologic structures with SPOT satellite data. AAPG (Am. Assoc. Pet. Geol.) Bull. 76 (1), 101–120.

Beroiz, C., Barón, A., Ramírez del Pozo, J., Giannini, G., Gervilla, M., 1972a. Mapa Geológico de España. Escala 1:50.000. Instituto Geológico y Minero de España, Madrid. Hoja: 30 Villaviciosa.

Beroiz, C., Ramírez del Pozo, J., Giannini, G., Barón, A., Julivert, M., Truyols, J., 1972b. Mapa Geológico de España. Escala 1:50.000. Instituto Geológico y Minero de España, Madrid. Hoja: 14 Gijón.

Blenkinsop, T.G., 2012. Visualizing structural geology: from Excel to Google Earth. Comput. Geosci. 45, 52–56.

Bradski, G., Kaehler, A., 2008. Learning OpenCV. Computer Vision with the OpenCV Library, p. 578.

Buckley, S.J., Howell, J.A., Enge, H.D., Kurz, T.H., 2008. Terrestrial laser scanning in geology: data acquisition, processing and accuracy considerations. J. Geol. Soc. 165 (3), 625–638.

Buckley, S.J., Howell, J.A., Naumann, N., Lewis, C., Chmielewska, M., Ringdal, K., Vanbiervliet, J., Bowei, T., Mulelid-Tynes, O.S., Foster, D., Maxwell, G., Pugsley, J., 2021. V3Geo: a cloud-based repository for virtual 3D models in geoscience. Geosci. Comm. Discuss. 1–27.

Bulnes, M., Poblet, J., de Ana, Á., Masini, M., 2016. Comportamiento de las calizas "griotte" carboníferas frente a deformaciones compresivas en dos localidades de la Zona Cantábrica (NO de la Península Ibérica): resultados preliminares. Trab. Geol. 36, 61–80.

Bulnes, M., Poblet, J., Uzkeda, H., Rodríguez-Álvarez, I., 2019. Mechanical stratigraphy influence on fault-related folds development: insights from the Cantabrian zone (NW Iberian Peninsula). J. Struct. Geol. 118, 87–103.

Carrivick, J.L., Smith, M.W., Quincey, D.J., 2016. Structure from Motion in the Geosciences. John Wiley & Sons, Chichester, p. 197.

Cawood, A.J., Bond, C.E., 2019. eRock: an open-access repository of virtual outcrops for geoscience education. GSA Today (Geol. Soc. Am.) 29 (2), 36–37.

Cawood, A.J., Bond, C.E., Howell, J.A., Butler, R.W.H., Totake, Y., 2017. LiDAR, UAV or compass-clinometer? Accuracy, coverage and the effects on structural models. J. Struct. Geol. 98, 67–82.

Corradetti, A., Tavani, S., Russo, M., Arbués, P.C., Granado, P., 2017. Quantitative analysis of folds by means of orthorectified photogrammetric 3D models: a case study from Mt. Catria, northern Apennines, Italy. Photogramm. Rec. 32 (160), 480–496.

De Ana, A., 2015. Estructura de los materiales paleozoicos entre las localidades de Llanes y Andrín (Unidad del Ponga, Zona Cantábrica). MSc Thesis, vol. 30. Universidad de Oviedo.

De Sitter, L.U., 1962. The structure of the southern slope of the Cantabrian Mountains. Geological map with section scale 1:100,000. Leidse Geol. Meded. 26, 255–264.

De Sitter, L.U., Van den Bosch, W.J., 1969. The structure of the SW part of the Cantabrian Mountains. Leidse Geol. Meded. 43 (1), 213–215.

Dhont, D., Luxey, P., Chorowicz, J., 2005. 3-D modeling of geologic maps from surface data. AAPG (Am. Assoc. Pet. Geol.) Bull. 89 (11), 1465–1474.

Dueholm, K.S., Garde, A.A., Pedersen, A.K., 1993. Preparation of accurate geological and structural maps, cross-sections or block diagrams from colour slides, using multi-model photogrammetry. J. Struct. Geol. 15 (7), 933–937.

Fernández, O., 2005. Obtaining a best fitting plane through 3D georeferenced data. J. Struct. Geol. 27 (5), 855–858.

Fernández, O., Muñoz, J.A., Arbués, P., Falivene, O., Marzo, M., 2004. Three-dimensional reconstruction of geological surfaces: an example of growth strata and turbidite systems from the Ainsa basin (Pyrenees, Spain). AAPG (Am. Assoc. Pet. Geol.) Bull. 88 (8), 1049–1068.

Fillon, C., Pedreira, D., Van Der Beek, P.A., Huismans, R.S., Barbero, L., Pulgar, J.A., 2016. Alpine exhumation of the central Cantabrian mountains, northwest Spain. Tectonics 35 (2), 339–356.

Flor, G., 1983. Las rasas asturianas: ensayos de correlación y emplazamiento. Trab. Geol. 13 (13), 65–83.

Fonstad, M.A., Dietrich, J.T., Courville, B.C., Jensen, J.L., Carbonneau, P.E., 2013. Topographic structure from motion: a new development in photogrammetric measurement. Earth Surf. Process. Landforms 38, 421–430.

Gallastegui, J., 2000. Estructura cortical de la cordillera y margen continental cantábricos: perfiles ESCI-N. Trab. Geol. 22, 3–234.
García-Ramos, J.C., Gutiérrez-Claverol, M., 1995. La cobertera mesozoico-terciaria. In: Aramburu, C., Bastida, F. (Eds.), Geología de Asturias. Ediciones Trea S.L., Gijón, pp. 81–94.
Gindraux, S., Boesch, R., Farinotti, D., 2017. Accuracy assessment of digital surface models from unmanned aerial vehicles' imagery on glaciers. Rem. Sens. 9, 186.
Granado, P., Tavani, S., Carrera, N., Muñoz, J.A., 2018. Deformation pattern around the Conejera fault blocks (Asturian basin, North Iberian margin). Geol. Acta 16 (4), 357–373.
Gutiérrez-Claverol, M., Fernández, C.L., Alonso, J.L., 2006. Procesos neotectónicos en los depósitos de rasa de la zona de Canero (Occidente de Asturias). Geogaceta 40, 75–78.
Gutiérrez-Claverol, M., Torres-Alonso, M., Luque-Cabal, C., 2002. El subsuelo de Gijón. Aspectos geológicos. CQ Licer S.L., Oviedo, p. 462.
Harwin, S., Lucieer, A., 2012. Assessing the accuracy of georeferenced point clouds produced via multi-view stereopsis from unmanned aerial vehicles (UAV) imagery. Rem. Sens. 4, 1573–1599.
Hodgetts, D., 2013. Laser scanning and digital outcrop geology in the petroleum industry: a review. Mar. Petrol. Geol. 46, 335–354.
Höfle, B., Vetter, M., Pfeifer, N., Mandlburger, G., Stötter, J., 2009. Water surface mapping from airborne laser scanning using signal intensity and elevation data. Earth Surf. Process. Landforms 34, 1635–1649.
Julivert, M., 1971. Décollement tectonics in the Hercynian cordillera of NW Spain. Am. J. Sci. 270, 1–29.
Julivert, M., 1983. La estructura de la Zona Cantábrica. In: Comba, J.A. (Ed.), Geología de España. Libro Jubilar J. M. Ríos, Tomo I. Instituto Geológico y Minero de España, Madrid, pp. 339–381.
Julivert, M., Fontboté, J.M., Ribeiro, A., Conde, L.E., 1972. Mapa Tectónico de la Península Ibérica y Baleares, Escala 1:1.000.000. Instituto Geológico y Minero de España, Madrid.
Lepvrier, C., Martínez-García, E., 1990. Fault development and stress evolution of the post-Hercynian Asturian Basin (Asturias and Cantabria, northwestern Spain). Tectonophysics 184 (3–4), 345–356.
Li, W., Bertin, S., Friedrich, H., 2018. Combining Structure from Motion and close-range stereo photogrammetry to obtain scaled gravel bar DEMs. Int. J. Rem. Sens. 39 (23), 1–25.
Lindberg, E., Holmgren, J., Olofsson, K., Wallerman, J., Olsson, H., 2013. Estimation of tree lists from airborne laser scanning using tree model clustering and k-MSN imputation. Rem. Sens. 5, 1932–1955.
Lisle, R.J., 2006. Google Earth: a new geological resource. Geol. Today 22 (1), 29–32.
López-Fernández, C., Pulgar, J.A., Gallart, J., González-Cortina, J.M., Díaz, J., Ruiz, M., 2004. Actividad sísmica en el noroeste de la Península Ibérica observada por la red sísmica local del Proyecto GASPI (1999-2002). Trab. Geol. 24, 91–107.
Lotze, F., 1945. Zur gliederung der varisziden der Iberischen Meseta. Geotekt. Forsch. 6, 78–92.
Marcos, A., 1968. La tectónica de la Unidad de La Sobia-Bodón. Trab. Geol. 2, 59–87.
Marquínez, J., 1989. Síntesis cartográfica de la Región del Cuera y los Picos de Europa. Trab. Geol. 18, 137–145.
Martín, S., García, S., Suárez, J., Rubio, R., Gallego, R., Morán, S., 2007. VISAGE: Estereoscopio virtual aplicado a la Geología. XII International Conference of Energy and Mineral Resources, Oviedo.
Martín, S., Pupo, L., Cabrera, Y., Rubio, R., 2011. An open-source C sharp library based on OpenGL for stereoscopic graphic applications development. In: Proceedings of the First International Conference on Simulation and Modeling Methodologies, Technologies and Applications, pp. 205–210.
Martín, S., Uzkeda, H., Poblet, J., Bulnes, M., 2019. Geological interpretation of two virtual outcrops of deformed Paleozoic rocks (NW Iberian Peninsula) using 3D stereo VDT in a computer assisted virtual environment (CAVE ™). J. Iber. Geol. 45, 565–584.
Martín, S., Uzkeda, H., Poblet, J., Bulnes, M., Rubio, R., 2013. Construction of accurate geological cross-sections along trenches, cliffs and mountain slopes using photogrammetry. Comput. Geosci. 51, 90–100.
Martínez-Álvarez, J.A., 1965. Rasgos geológicos de la zona oriental de Asturias. Instituto de Estudios Asturianos, Diputación Provincial de Oviedo, p. 132.
Martínez-Álvarez, J.A., Gutiérrez-Claverol, M., Vargas-Alonso, I., 1968. Esquema geológico de la zona de la Cordillera Cantábrica comprendida entre los Puertos "Pajares" y "Ventana" (Asturias-León). Escuela de Minas, Universidad de Oviedo.
Martínez-García, E., 1980. Mapa geológico de España. Escala 1:50.000. Instituto Geológico y Minero de España, Madrid. Hoja: 32 Llanes.
Martínez-García, E., Corrales, I., Valladares, I., Méndez, I., Ramírez del Pozo, J., van Ginkel, A.C., Lamolda, M., Moreno de Castro, E., Marcos, A., 1981. Memoria del mapa geológico de España. Escala 1:50.000. Instituto Geológico y Minero de España, Madrid, p. 40. Hoja: 32 Llanes.
Mary, G., 1983. Evolución del margen costero de la Cordillera Cantábrica en Asturias desde el Mioceno. Trab. Geol. 13, 3–37.
Masini, M., Poblet, J., Bulnes, M.T., 2010a. Structural analysis and deformation architecture of a fault-propagation fold in the southern Cantabrian Mountains, NW Iberian Peninsula. Trab. Geol. 30, 55–62.
Masini, M., Bulnes, M., Poblet, J., 2010b. Cross-section restoration: a tool to simulate deformation. Application to a fault-propagation fold from the Cantabrian fold and thrust belt, NW Iberian Peninsula. J. Struct. Geol. 32 (2), 172–183.
McCaffrey, K.J.W., Hodgetts, D., Howell, J., Hunt, D., Imber, J., Jones, R.R., Tomasso, M., Thurmond, J., Viseur, S., 2010. Virtual fieldtrips for petroleum geoscientists. In: Vining, B.A., Pickering, S.C. (Eds.), Petroleum Geology: from Mature Basins to New Frontiers. Proceedings of the 7th Petroleum Geology Conference, pp. 19–26. London.
Merino-Tomé, O., Suárez-Rodríguez, A., Alonso, J.L., 2014. Mapa Geológico Digital Continuo a Escala 1:50.000 de la Zona Cantábrica (Plan GEODE). http://info.igme.es/visor web.
Navarro-Vázquez, D., Rodríguez-Fernández, R., 1978. Mapa geológico de España. Escala 1:50.000. Instituto Geológico y Minero de España, Madrid. Hoja: 101 Villablino.
Navarro-Vázquez, D., , ENADIMSA, Departamento de Paleontología de la Universidad de Oviedo, Rodríguez-Fernández, R., 1982. Memoria del Mapa Geológico de España. Escala 1:50.000. Hoja: 101 Villablino, vol. 56. Instituto Geológico y Minero de España, Madrid.
Novakova, L., Pavlis, T.L., 2017. Assessment of the precision of smart phones and tablets for measurement of planar orientations: a case study. J. Struct. Geol. 97, 93–103.
Novakova, L., Pavlis, T.L., 2019. Modern methods in structural geology of twenty-first century: digital mapping and digital devices for the field geology. In: Mukherjee, S. (Ed.), Teaching Methodologies in Structural Geology and Tectonics. Springer, Singapore, pp. 43–54.
Odriozola, M., 2016. Extensión y compresión en los materiales jurásicos de la playa de Peñarrubia. Gijón. MSc Thesis, Universidad de Oviedo, p. 31.
Oniga, V.-E., Breaban, A.-I., Statescu, F., 2018. Determining the optimum number of ground control points for obtaining high precision results based on UAS images. Multidiscip. Digit. Publish. Inst. Proc. 2 (7), 352.
Otepka, J., Ghuffar, S., Waldhauser, C., Hochreiter, R., Pfeifer, N., 2013. Georeferenced point clouds: a survey of features and point cloud management. ISPRS Int. J. Geo-Inf. 2, 1038–1065.
Pérez-Estaún, A., Bastida, F., 1990. Cantabrian zone: structure. In: Dallmeyer, R.D., Martínez-García, E. (Eds.), Pre-Mesozoic Geology of Iberia. Springer-Verlag, Berlin, pp. 55–69.
Pérez-Estaún, A., Bastida, F., Alonso, J.L., Marquínez, J., Álvarez-Marrón, J., Marcos, A., Pulgar, J.A., 1988. A thin-skinned tectonics model for an arcuate fold and thrust belt: the Cantabrian Zone (Variscan Ibero-Armorican Arc). Tectonics 7, 517–537.
Pignatelli, R., Giannini, G., Ramírez del Pozo, J., Beroiz, C., Barón, A., 1972. Mapa Geológico de España. Escala 1:50 000, Hoja: 15 Lastres. Instituto Geológico y Minero de España, Madrid.
Poblet, J., Bulnes, M., Uzkeda, H., Magán, M., 2022. Using the Schmidt hammer on folds: An example from the Cantabrian Zone (NW Iberian Peninsula). J. Struct. Geol. 155, 104512.
Pringle, J.K., Westerman, A.R., Clark, J.D., Drinkwater, N.J., Gardiner, A.R., 2004. 3D high-resolution digital models of outcrop analogue study sites to constrain reservoir model uncertainty: an example from Alport Castles, Derbyshire, UK. Petrol. Geosci. 10 (4), 343–352.
Pulgar, J.A., Alonso, J.L., Espina, R.G., Marín, J.A., 1999. La deformación alpina en el basamento varisco de la Zona Cantábrica. Trab. Geol. 21, 283–294.
Ramsay, J.G., 1967. Folding and Fracturing of Rocks. Mc Graw Hill Book Company, New York, p. 568.
Rodríguez-Fernández, L.R., Barba, P., Fernández, L.P., Bardají, T., Silva, P.G., Suárez Rodríguez, A., Heredia, N., Gallastegui, G., Paniagua, A., Galán, L., Martínez-Álvarez, J.A., Torres Alonso, M., Gutiérrez Claverol, M., López Díaz, F., Toyos, J.M., Villa, E., Salvador González, C., Bravo Fernández, I., 1991. Memoria del mapa geológico de España. Escala 1:50.000. Hoja: 102 Los Barrios de Luna. Instituto Tecnológico GeoMinero de España, Madrid, p. 130.
Savage, J.F., 1979. The Hercynian orogeny in the Cantabrian mountains, northern Spain. Krystalinikum 14, 91–108.
Savage, J.F., 1981. Geotectonic cross-section through the Cantabrian mountains, northern Spain. Geol. Mijnbouw 81, 3–5.
Sørensen, E.V., Dueholm, M., 2018. Analytical procedures for 3D mapping at the photogeological laboratory of the geological survey of Denmark and Greenland. Geol. Surv. Den. Greenl. Bull. 41, 99–104.
Sørensen, E.V., Guarnieri, P., 2018. Remote geological mapping using 3D photogrammetry: an example from Karrat, West Greenland. Geol. Surv. Den. Greenl. Bull. 41, 63–66.
Suárez-Rodríguez, A., Toyos, J.M., López-Díaz, F., Heredia, N., Rodríguez-Fernández, L. R., Gutiérrez-Alonso, G., 1991. Mapa geológico de España. Escala 1:50.000. Hoja: 102 Los Barrios de Luna. Instituto Tecnológico y Geominero de España, Madrid.
Suárez-Vega, L.C., 1974. Estratigrafía del Jurásico de Asturias. Cuad. Geol. Iber. 74 (3), 1–369.
Svennevig, K., Guarnieri, P., Stemmerik, L., 2015. From oblique photogrammetry to a 3D model – structural modeling of Kilen, eastern North Greenland. Comput. Geosci. 83, 120–126.
Tavani, S., Corradetti, A., Billi, A., 2016. High precision analysis of an embryonic extensional fault-related fold using 3D orthorectified virtual outcrops: the viewpoint importance in structural geology. J. Struct. Geol. 86, 200–210.
Tavani, S., Granado, P., Corradetti, A., Girundo, M., Iannace, A., Arbués, P., Muñoz, J.A., Mazzoli, S., 2014. Building a virtual outcrop, extracting geological information from it, and sharing the results in Google Earth via OpenPlot and Photoscan: an example from the Khaviz Anticline (Iran). Comput. Geosci. 63, 44–53.
Torres-Sánchez, J., López-Granados, F., Borra-Serrano, I., Peña, J.M., 2017. Assessing UAV-collected image overlap influence on computation time and digital surface model accuracy in olive orchards. Precis. Agric. 19 (1), 115–133.
Triggs, B., McLauchlan, P.F., Hartley, R.I., Fitzgibbon, A.W., 2000. Bundle adjustment—a modern synthesis. In: Triggs, B., Zisserman, A., Szeliski, R. (Eds.), Vision Algorithms: Theory and Practice. Springer-Verlag, Berlin, pp. 298–372.
Trinks, I., Clegg, P., McCaffrey, K., Jones, R., Hobbs, R., Holdsworth, B., Holiman, N., Imber, J., Waggott, S., Wilson, R., 2005. Mapping and analysing virtual outcrops. Vis. Geosci. Annu. Arch. 10 (1), 13–19.

Uzkeda, H., 2013. Reconstrucción 3D y análisis estructural de las rocas jurásicas de Colunga-Tazones (Cuenca Asturiana, NO de la Península Ibérica). PhD Thesis. Universidad de Oviedo, p. 244.
Uzkeda, H., Bulnes, M., Poblet, J., García-Ramos, J.C., Piñuela, L., 2013. Buttressing and reverse reactivation of a normal fault in the Jurassic rocks of the Asturian Basin, NW Iberian Peninsula. Tectonophysics 599, 117–134.
Uzkeda, H., Bulnes, M., Poblet, J., García-Ramos, J.C., Piñuela, L., 2016. Jurassic extension and Cenozoic inversion tectonics in the Asturian Basin, NW Iberian Peninsula: 3D structural model and kinematic evolution. J. Struct. Geol. 90, 157–176.
Uzkeda, H., Poblet, J., Bulnes, M., Martín, S., 2018. Effects of inherited structures on inversion tectonics: examples from the Asturian basin (NW Iberian Peninsula) interpreted in a computer assisted virtual environment (CAVE). Geosphere 14 (4), 1635–1656.
Valenzuela, M., García-Ramos, J.C., Suárez de Centi, C., 1986. The Jurassic sedimentation in Asturias (N Spain). Trab. Geol. 16, 121–132.
Wellmann, F., Schaaf, A., de la Varga, M., von Hagke, C., 2019. From Google Earth to 3D geology problem 2: seeing below the surface of the digital Earth. Dev. Struct. Geol. Tect. 5, 189–204.
Wu, C., 2013. Towards linear-time incremental structure from motion. In: Proceedings of the International Conference on 3D Vision, vol. 2013, pp. 127–134. Seattle.
Wu, C., Agarwal, S., Curless, B., Switz, S.M., 2011. Multicore bundle adjustment. Proc. Comput. Vis. Theory Appl. 2011, 3057–3064. Colorado Springs.
Xu, X., Aiken, C.L., Bhattacharya, J.P., Corbeanu, R.M., Nielsen, K.C., McMechan, G.A., Abdelsalam, M.G., 2000. Creating virtual 3-D outcrop. Lead. Edge 19 (2), 197–202.
Xu, X., Bhattacharya, J.P., Davies, R.K., Aiken, C.L.V., 2001. Digital geologic mapping of the Ferron sandstone, muddy Creek, Utah, with GPS and reflectorless rangefinder. GPS Solut. 19 (1), 15–23.